Title: Selective translation by alternative bacterial ribosomes

Authors: Yu-Xiang Chen[1a], Zhi-yu Xu[2a], Bi-Wei Wang[1], Xueliang Ge[3], Jun-Hao Zhu[4], Suparna Sanyal[3], Zhi John Lu[2*], Babak Javid[1*]

Affiliations:

[1] Centre for Global Health and Infectious Diseases, Collaborative Innovation Centre for the Diagnosis and Treatment of Infectious Diseases, Tsinghua University School of Medicine, Beijing, China

[2] MOE Key Laboratory of Bioinformatics, Center for Synthetic and Systems Biology, School of Life Sciences, Tsinghua University, Beijing, China

[3] Department of Cell and Molecular Biology, Uppsala University, Sweden

[4] Immunology and Infectious Diseases, Harvard Chan School of Public Health, Boston, USA

[a] These authors contributed equally to this work

* to whom correspondence should be addressed:

ZJL: zhilu@tsinghua.edu.cn

BJ: bjavid@gmail.com (lead contact)

Summary

Alternative ribosome subunit proteins are prevalent in the genomes of diverse microbial species, but their functional significance is controversial, partly due to lack of direct comparison of alternate ribosomal isoforms isolated from identical cellular contexts. Here, by simultaneously tagging and purifying canonical and alternative ribosomes in *Mycobacterium smegmatis*, we show that alternative ribosomes have distinct translational features compared with their canonical counterparts. Ribosome profiling revealed that translation by alternative ribosomes is characterized by a 5' polarity shift and altered codon preference, as well as differential translation of a subset of genes. Although alternative and canonical ribosomes have similar activity in peptide synthesis, alternative ribosomes showed a relative defect in initiation. Genetic interaction studies of the alternate ribosome operon with the mycobacterial genome by insertional transposon mutagenesis and deep sequencing identified synthetic lethal interactions that verified the distinct and non-redundant contribution of alternative ribosomes, including an unexpected role in iron homeostasis.

Keywords: ribosome heterogeneity, alternative ribosomes, specialized ribosomes, ribosome profiling, mycobacterium, adaptive translation, transposon insertion sequencing, Tnseq

Introduction

Ribosomes are the macromolecular machines that translate the genetic code into functional proteins (Jobe et al., 2019; Ramakrishnan, 2014; Rodnina, 2018). Shortly after their discovery and role in gene translation, the "one gene, one mRNA, one ribosome" hypothesis was proposed (Crick, 1958), but was quickly disproven (Brenner et al., 1961). This led in turn to the "homogeneity hypothesis" for ribosomes: that all ribosomes were identical macromolecules, that would translate all mRNAs with equal efficiency (Moore et al., 1968). However, observations that ribosome composition varied according to environmental conditions and other variables, immediately challenged the homogeneity hypothesis (Deusser and Wittmann, 1972). But until recently, the functional significance of ribosome heterogeneity has not been well understood.

In eukaryotic systems, there is increasing evidence for the role and importance of ribosomal heterogeneity in fundamental physiology, development and disease, in systems from budding yeast, to organelles and animals (Genuth and Barna, 2018a, b; Gerst, 2018; Parenteau et al., 2015). In particular, specialized ribosomes have been shown to be important for vitamin B12 transport and cell-cycle components (Shi et al., 2017), hematopoiesis (Zhang et al., 2013) and development (Kondrashov et al., 2011). Mutations in ribosomal proteins, or haploinsufficiency of their coded genes have been implicated in a number of disorders such as the ribosomopathies (Genuth and Barna, 2018b; Warren, 2018). Our understanding of ribosomal heterogeneity in bacteria is less advanced (Byrgazov et al., 2013). Using high-fidelity mass spectrometry of intact 70S ribosomes from *Escherichia coli* revealed considerable heterogeneity, such as the presence or absence of the stationary-phase-induced ribosomal-associated protein, SRA (van de Waterbeemd et al., 2017). Other studies implicating specialized bacterial ribosomes (Kaberdina et al., 2009; Vesper et al., 2011) have recently been questioned (Culviner and Laub, 2018; Lange et al., 2017; Mets et al., 2019). Nonetheless, it is intriguing to speculate that specialized bacterial ribosomes, generated in

response to environmental stressors, would result in altered translation, which in turn might allow adaptation to the stressful environment (Byrgazov et al., 2013).

Specialized ribosomes could be generated via changes in the stoichiometry of canonical ribosomal components, association of accessory ribosomal proteins, modification of ribosomal rRNA or incorporation of alternative ribosomal subunits, coded by paralogous or homologous genes (reviewed in (Dinman, 2016; Genuth and Barna, 2018b)). Most eukaryotic organisms code for paralogues of ribosomal subunit genes, and around half of sequenced bacterial genomes from one study included at least one ribosomal protein paralogue (Yutin et al., 2012). One well-characterized group of paralogous ribosomal proteins are those that lack cysteine-rich motifs (C-) compared with canonical cysteine-containing homologues (C+). C- paralogues have been described in many bacteria, including mycobacteria (Makarova et al., 2001; Prisic et al., 2015; Tobiasson et al., 2019). In mycobacteria, the conserved alternative C- ribosomal subunits are coded in a single operon regulated by a zinc uptake regulator (zur), which represses expression in the presence of zinc ions (Gaballa et al., 2002), and has led to the suggestion that the function for C-/C+ ribosomal subunit paralogues is to allow for dynamic storage of zinc (Akanuma et al., 2006; Gabriel and Helmann, 2009; Nanamiya et al., 2004). Furthermore, although these alternative mycobacterial ribosomal proteins (AltRPs) have recently been demonstrated to incorporate into assembled ribosomes (Li et al., 2018a), their participation in gene translation has been called into question (Li et al., 2018a). Here, we demonstrate convincingly using a fully reconstituted mycobacterial translation system that ribosomes containing the alternative subunit RpsR2 (AltRpsR) actively translate. Furthermore, the translational landscape as measured by ribosome profiling of these alternative mycobacterial ribosomes are distinct from those generated by canonical ribosomes purified from the same cell and are characterized by a 5' polarity shift. Conditional essentiality analysis of wild-type *M. smegmatis* and a strain lacking the AltRP operon reveals significant synthetically lethal interactions of the AltRP operon with the mycobacterial

genome and identifies a potential role for alternative ribosomes in iron homeostasis, thus demonstrating a non-redundant role for alternative ribosomes under nutrient stress.

Results

Alternative mycobacterial ribosomes engage in gene translation

Mycobacteria encode for several alternative C- ribosomal proteins, four of which are conserved throughout the genus and are encoded within one operon (Li et al., 2018a; Prisic et al., 2015). All four of these are annotated as *in vitro* "non-essential", and we therefore deleted the operon in *M. smegmatis* via a double cross-over homologous recombination strategy (Su et al., 2016), resulting in the strain *M. smegmatis*-ΔAltRP (ΔAltRP). As previously demonstrated, this strain grew normally in zinc-replete 7H9 complete medium (Fig. S1A). However, the strain had a significant growth defect when cultured in relatively zinc-deplete Sauton's medium, and the defect was partially rescued when the operon was complemented (Fig. S1A). We wished to biochemically characterize alternative ribosome (AltRibo) function by purifying ribosomes containing alternative or canonical subunit proteins. We chose to C-terminally tag RpsR2 (AltRpsR) with 3xFLAG, since of the four alternative ribosome genes within the operon, the C-terminus of RpsR showed the greatest sequence variation (Fig. 1A), and we reasoned that it therefore was most likely to tolerate tagging. Following complementation of the ΔAltRP strain with FLAG-tagged AltRpsR, we performed affinity purification using anti-FLAG-specific antibody (Fig. S1B). SDS-PAGE analysis showed a staining pattern similar to canonical 70S ribosomes purified from the ΔAltRP strain via conventional sucrose density gradient ultracentrifugation (Fig. S1B,C). Mass-spectrometry analysis of the protein bands confirmed that pull-down of AltRpsR co-precipitated all ribosomal protein subunits (Table S1), suggesting that affinity tagging and purification of alternative and canonical ribosomes could be achieved by tagging RpsR.

To investigate alternative (AltRibo) and canonical (CanRibo) ribosome function within the same cellular context, we constructed a strain of *M. smegmatis* in which both RpsR subunits had affinity tags inserted at their C-terminus, at their native loci on the mycobacterial chromosome (Fig. 1B and see Methods). Immunoblotting of total cell-lysate and purified ribosomes confirmed earlier observations (Prisic et al., 2015) that AltRpsR is repressed in zinc-replete medium, and its expression is up-regulated upon zinc depletion (Fig. 1C). However, there is considerable debate regarding whether AltRPs are components of functional, translating ribosomes (Keren et al., 2011; Li et al., 2018b; Prisic et al., 2015). To address this, we purified the polysome fraction of our dual-tagged strain and affinity purified AltRibos by FLAG-IP. The fraction was split and one aliquot was subjected to extensive endonuclease digestion with micrococcus nuclease (MNase), which specifically degrades nucleic acid not protected by ribosomes ((Becker et al., 2013) and Fig. 1D). Following digestion, the pull-down products were subjected to immunoblotting by both anti-FLAG and anti-HA antibodies, detecting AltRpsR and canonical RpsR (CanRpsR) respectively. We reasoned that if AltRibos and CanRibos are both resident on the same translating polysome, lack of MNase digestion should purify both components, whereas extensive digestion of polysomes to monosomes by MNase would result in affinity purification predominantly of just AltRibos. This was confirmed by our results (Fig. 1D), suggesting that AltRibos are resident on polysomes comprised of both AltRibos and CanRibos, supporting their active role in gene translation.

To further characterize whether AltRibos are able to translate, we subjected affinity purified AltRibos to biochemical analysis in a mycobacterial cell-free translation system (Li et al., 2018b). AltRibos were able to synthesise di-peptides at similar efficiency to CanRibos (Fig. 1E), confirming that AltRibos are capable of gene translation.

Alternative mycobacterial ribosomes have distinct translational profiles compared with canonical ribosomes

Having demonstrated that AltRibos actively function in gene translation, we wanted to determine whether the translational landscapes generated by AltRibos differed from CanRibos. Our dual-RpsR-tagged strain permitted us to interrogate selective ribosome translation profiles from the same cellular population, which would eliminate potential differences due to mRNA abundance or other confounding factors (Becker et al., 2013; Oh et al., 2011). However, since AltRpsR was FLAG-tagged and CanRpsR was HA-tagged (Strain A), there remained the formal possibility that any differences observed on the ribosome profiles might be due to interference of the specific tag. To control for this, we generated a second dual-tagged strain in which the affinity tags were swapped, i.e. FLAG-tagged CanRpsR and HA-tagged AltRpsR (Strain B – Fig. 2A). The regulation of AltRpsR and CanRpsR was similarly regulated in zinc-replete and zinc-deplete conditions (Fig. S2A), confirming that Strain B had comparable physiology with Strain A.

We subjected affinity-purified ribosomes from both strains to ribosome profiling as previously described, with minor modifications ((Becker et al., 2013; Elgamal et al., 2014; Ingolia et al., 2012; Shell et al., 2015), Fig. 2A and see Methods). We grew the strains in relatively zinc-replete conditions, which allowed cultures to grow to greater density for ribosome isolation. Under these conditions, the majority of ribosomes were CanRibos. Immunoblotting confirmed that our isolation work-flow was efficient at enriching both types of ribosomes (Fig. 2B). We performed ribosome profiling with two independent replicates, which showed a high degree of reproducibility (Fig. S2B). Furthermore, position analysis of aligned reads revealed a clear 3 nucleotide periodicity (Fig. S3A, B), confirming that our reads were derived from translating ribosomes for both AltRibos and CanRibos. Comparing the genome-wide translational profiles generated by AltRibos and CanRibos, CanRibo-derived reads were highly correlated with total ribosome input, consistent with the fact that the majority of ribosomes under the tested condition

were CanRibos (Fig. 2C). However, the reads generated from AltRibos were less well correlated with the total ribosomal input, suggesting that translational profiles from AltRibos were distinct from CanRibos (Fig. 2C). Regardless of affinity tag, CanRibo- and AltRibo-derived reads were highly correlated with each other when comparing translational efficiency profiles generated by Strain A and Strain B (Fig. 2D), following correction for mRNA expression by paired RNA-seq (Fig. S4). These data together strongly support that the differences in translational profiles from AltRibos were due to intrinsic differences in the translational landscape generated by AltRibos.

Alternative ribosome profiles have polarized read distributions and differential codon usage

Our analysis of differences in translational profiles between canonical and alternative mycobacterial ribosomes revealed that for translation of certain genes, there were clear differences in the distribution of sequencing reads along the gene length between the two samples, for example for translation of *Msmeg_0363* (Fig. 3A). To characterize these differences on a genome-wide basis, we calculated the polarity score to determine the distribution of aligned reads for each coding gene (Schuller et al., 2017). Polarity scores between -1 and 0 represent read accumulation at the 5' end of the coding region, and between 0 and +1 represent read accumulation at the 3' end of the coding region (see Methods). To avoid noise generated by read accumulation around the start and stop codons, we excluded the first and last 15 nucleotides in our analysis (Schuller et al., 2017). Comparing the polarity score of AltRibos with CanRibos and total ribosome input from both Strain A and Strain B, there was a clear polarity shift towards a 5' read accumulation in alternative ribosomes (Fig. 3B).

Translation elongation does not proceed at a uniform pace (Li et al., 2012; Loayza-Puch et al., 2016; Nedialkova and Leidel, 2015; Novoa and Ribas de Pouplana, 2012). We investigated whether alternative and canonical ribosomes differed in codon-reading rates. AltRibos from either Strain A or Strain B showed similar codon usage pattern across all 61 sense codons (Fig.

4A, B). Comparing CanRibos with AltRibos with total ribosome input across all coding genes, there were significant differences in codon usage between the two ribosome isoforms in both Strain A (Fig. 4C) and Strain B (Fig. 4D). From our analysis of all 61 sense codons in both strains, 12 showed relatively high occupancy in AltRibos compared with total ribosomes, and 12 showed relatively low occupancy (Fig. 4E). We wished to determine whether altered codon usage might be associated with the observed polarity differences between AltRibos and CanRibos. We considered the first and last 50 codons of all coding genes and compared the relative abundance of the 12 high- and 12 low-occupancy codons in these regions. For the 12 high occupancy codons, 10 were relatively enriched at the 5' end of coding regions, and for the 12 low occupancy codons, 8 were relatively enriched at the 3' end of coding regions (Fig. 4F), potentially suggesting a mechanism for the observed polarity differences between alternative and canonical ribosomes. Furthermore, although purified AltRibos formed 70S initiation complexes, they appeared to do so at slightly lower efficiency compared with CanRibos (Fig. 4G), suggesting another potential mechanism for the observed 5' polarity shift. The lower efficiency in 70S initiation complex formation could be due to impaired binding of the initiator tRNA as demonstrated by BODIPY-Met-tRNA^{fMet} binding to the programmed ribosome monitored by increase in BODIPY fluorescence (Fig. 4H).

Alternative ribosomes have bias for the translation of a subset of genes

Our data suggested that alternative ribosomes had intrinsic differences in gene translation compared with canonical ribosomes. Did these differences result in distinct translational profiles of a subset of genes? To address this, we performed differential expression analysis on AltRibo- and CanRibo-generated ribosome profile datasets, and compared these with the total ribosome input. As expected, there were few differences between CanRibos and total ribosomes (Fig. 5A), since the majority of ribosomes in the total pool were canonical ribosomes. By contrast, there were a large number of genes that were translated with either decreased or increased preference

by AltRibos compared with the total ribosome input (Fig. 5B). Of note, there was relatively little overlap in the up-regulated gene set when comparing Strain A and Strain B – representing FLAG- and HA-tagged AltRpsR respectively. However, there was substantial enrichment of under-represented genes between the two strains (Fig. 5C). Consistent with this, comparing all 8 biological replicates in both strains, low-efficiency translated gene sets were highly similar in all 4 AltRibo datasets (Fig. 5D). To determine whether high or low efficiency translated genes belonged to functional groups, we performed gene ontology analysis. Examining the top enriched gene sets from both Strain A and Strain B, there were no gene sets enriched for both strains in the high efficiency translated genes, but low efficiency translated genes were enriched for 'growth' and membrane proteins (Fig. 5E, Fig. S5).

Transposon insertion sequencing reveals a role for the alternative ribosome operon in iron homeostasis

Our data suggested the translational landscape of mycobacterial ribosomes were distinct from canonical ribosomes, and that these differences were due to intrinsic altered properties of the ribosomes in translating the mycobacterial genome. Although alternative ribosomes represented the minority ribosome population under standard laboratory growth conditions, there is evidence that the operon is significantly upregulated in physiologically relevant conditions such as infection and antibiotic exposure (Keren et al., 2011; Li et al., 2018a), and under zinc depletion *in vitro*, the alternative ribosomes represent the majority population (Dow and Prisic, 2018; Li et al., 2018a; Prisic et al., 2015). To investigate the potential genetic interactions of the operon with the mycobacterial genome, we generated large transposon-mutagenized libraries of *M. smegmatis* on both a wild-type and ΔAltRP background (see Methods). We then performed deep-sequencing of the transposon-insertion sites (Tnseq) on two independent libraries generated on each background, which allows us to comprehensively determine conditional essentiality of all genes within the genome (Baranowski et al., 2018; Kieser et al., 2015). We performed Tnseq analysis in both

zinc-replete and zinc-deplete conditions. For zinc-depletion, we used the intra-cellular ion chelator N,N,N,N'-tetrakis(2-pyridinylmethyl)-1,2-ethanediamine (TPEN), which chelates transition metals, including zinc, and has been used previously to upregulate the alternate ribosomal operon (Dow and Prisic, 2018; Li et al., 2018a). At a concentration of 10µg/ mL on 7H10 plates, TPEN significantly upregulated AltRpsR and down-regulated CanRpsR, without affecting bacterial growth and plating efficiency (Fig. 6A) and this concentration was used for selection of the transposon-mutagenized libraries under zinc depletion.

Under conditions of zinc-depletion, the previously dispensable AltRP genes become relatively conditionally essential in wild-type *M. smegmatis* (Fig. 6B and dataset S1). Upon zinc depletion, the number of conditionally essential genes in strain ΔAltRP compared with wild-type *M. smegmatis* substantially increased (Fig. 6B, C), verifying the non-redundant role of alternative ribosomes in particular in environmental conditions in which the operon is usually expressed. We examined which genes were differentially essential specifically in ΔAltRP during zinc depletion and identified *mbtN* (*M_smeg 2130*). Inspection of the number of transposon insertions at TA loci throughout the *mbtN* gene under the four conditions revealed that, except for the last TA locus, which tolerated insertions, *mbtN* could not tolerate insertions (i.e. was essential) in both wild-type *M. smegmatis* and ΔAltRP in the absence of zinc depletion. In the presence of zinc depletion, however, the gene could tolerate multiple transposon insertions throughout its length only in wild-type *M. smegmatis*, but remained intolerant of insertions in ΔAltRP (Fig. 6D). *mbtN* has been annotated as coding for the first step in mycobactin synthesis, a mycobacteria-specific siderophore (Madigan et al., 2015). These data suggested that under conditions in which AltRibos are expressed, i.e. zinc depletion, *mbtN* is no longer essential, but only if the AltRP operon is present. These data suggested a role for AltRibos in iron homeostasis. We therefore compared growth of wild-type *M. smegmatis*, the ΔAltRP strain and ΔAltRP complemented with the AltRP operon in medium that had iron removed by chelex 100 (Siegrist et al., 2009). The

ΔAltRP strain had a major growth defect compared with the wild-type and complemented strains in lag and logarithmic phases under these conditions (Fig. 6E). Since chelex 100 also binds zinc ions, we tested whether zinc or iron supplementation could specifically rescue growth. Although supplementation with zinc had a minor effect on growth, supplementation with iron alone completely rescued the growth defect and even allowed growth to a greater density than wild-type *M. smegmatis*, suggesting a specific iron-limiting phenotype for mycobacteria lacking alternative ribosomes (Fig. 6E).

Discussion

Together, our studies demonstrate that alternative mycobacterial ribosomes incorporating C-paralogues are not only competent for translation, but that these alternative ribosomes have distinct translational landscapes compared with their canonical counterparts. We leveraged the power of ribosome profiling and affinity purification of specialized ribosomes to show that alternative mycobacterial ribosomes, containing AltRpsR have altered codon usage compared with ribosomes containing the canonical RpsR paralogue, as well as a relative 5' polarity shift in translation of open reading frames. Ribosomal profiling of specialized ribosomes had previously demonstrated specific functions of heterogeneous ribosome populations in stem cells and for the translation of mitochondrial proteins in eukaryotic cells (Segev and Gerst, 2018; Shi et al., 2017). In bacteria, ribosome profiling of trigger factor associated with ribosomes demonstrated the requirement of trigger factor particularly for the translation of outer-membrane proteins in *E. coli* (Oh et al., 2011), but ribosome profiling had not been employed for ribosomes incorporating ribosomal protein paralogues.

There have been relatively few studies of bacterial ribosomal heterogeneity when compared with eukaryotic systems (Byrgazov et al., 2013). Two studies identified *E. coli* ribosomes specialized for the translation of leaderless mRNAs (Kaberdina et al., 2009; Vesper et al., 2011), but these

findings have been recently challenged (Chaudhuri et al., 2018; Culviner and Laub, 2018; Lange et al., 2017; Mets et al., 2019). However, there is evidence that ribosomal heterogeneity may be just as pervasive in bacteria as eukaryotes (Kurylo et al., 2018; Song et al., 2019). Mycobacteria, for example, have very distinct translational features compared with the model *E. coli* system (Cortes et al., 2013; Sawyer et al., 2018; Shell et al., 2015). Recent structural information about the mycobacterial ribosome identified new ribosomal protein subunits, but these new subunits, bL37 and bS22 were not present in all ribosomes identified by cryo-electron microscopy (Hentschel et al., 2017; Li et al., 2018b; Yang et al., 2017). Intriguingly, in our synthetic lethality screen, bL37, coded by *M_smeg 1916* is non-essential in wild-type *M. smegmatis*, but becomes essential in ΔAltRP under conditions of zinc-depletion (dataset S1). These genetic interaction data suggest that AltRibos and bL37-containing CanRibos may function in similar pathways.

Many diverse bacterial species code for C- ribosomal subunit paralogues (Yutin et al., 2012), but their distinct translational functions, if any, have not been fully characterized. A recent examination of the mycobacterial C- paralogues that are the subject of this study suggested that the C- ribosomes are hibernating and do not actively engage in gene translation(Li et al., 2019; Li et al., 2018a). Those findings are in stark contradistinction with our own. By both biochemical analysis and ribosome profiling, our data support a role for translating AltRibos. Furthermore, Ojha and colleagues suggested an exclusive association of a ribosomal hibernation promoting factor (*Msmeg_1878* and named MPY by them) with C- ribosomes. It is possible that use of supra-physiological (1mM) zinc in culture medium led to lack of binding of MPY to canonical (C+) ribosomes under those conditions (Li et al., 2018a). However, our isolation of ribosomes from *M. smegmatis*-ΔAltRP (where C- ribosomes would be absent by definition) by standard methods in standard growth medium (Table S1) as well as a previous study of *M. smegmatis* grown under conditions where C- ribosomes would not have been predominant (Trauner et al., 2012) suggest that MPY is not exclusively associated with C- ribosomes. Methodology resulting

in exclusive association of MPY with C- ribosomes, which would promote generalized ribosome hibernation (Gohara and Yap, 2018) might explain Li *et al's* results.

Our data suggest that alternative ribosomes and canonical ribosomes have differences potentially in both translation initiation and codon usage – both of which may contribute to the relative 5' polarity shift of reads in alternative ribosomes. Multiple mechanisms have been proposed for observed differences in elongation rates (Novoa and Ribas de Pouplana, 2012) including the presence of internal mRNA sequences, such as anti-Shine Dalgarno sequences (Li et al., 2012). Decoding of modified tRNA bases (Nedialkova and Leidel, 2015) and differential affinity of specific ribosome isoforms for aminoacyl-tRNAs (Loayza-Puch et al., 2016) also contribute to altered rates of gene translation. Of note, RpS18 (of which AltRpsR and CanRpsR are the two mycobacterial isoforms) is part of an mRNA "nest", which contributes to preinitiation binding of mRNA to the 30S subunit (Marzi et al., 2007), and it is tempting therefore to speculate that differences in RpsR protein sequence may contribute the observed differences in initiation complex formation.

Upon encountering physiologically relevant stressors, mycobacteria upregulate the alternative subunit operon. Our synthetic lethality data identifies both physiological advantages and liabilities associated with such a shift. In particular, we identified that *mbtN* is no longer essential in *M. smegmatis* under zinc depletion, but only if the alternative ribosomal operon is present. MbtN is an acyl-coA dehydrogenase that is involved in mycobactin synthesis (Chai et al., 2015; Madigan et al., 2015). Growth of the ΔAltRP strain was severely compromised when iron and other transition metals were removed from growth medium, but could be fully rescued by the sole addition of iron, but not zinc. The precise mechanisms by which expression of alternative ribosomes dispenses with MbtN and its potential role in iron homeostasis are unknown. *Mycobacterium smegmatis* has at least two siderophore synthesis pathways (Siegrist et al., 2009),

and it is possible that AltRibos may be involved in an alternative siderophore synthesis pathway that may bypass mycobactin. Our study reveals not only that alternative mycobacterial ribosomes actively participate in gene translation, but also provides evidence that gene translation by specialized ribosomes in bacteria contribute to environmental adaptation.

Acknowledgements

We thank Jianhuo Fang from the Tsinghua genomic and synthetic biology core for help in preparing the ribosome profile libraries. We would like to thank Eric Rubin and Hesper Rego for reading and commenting on the draft manuscript. This work was in part funded by grants from the Bill and Melinda Gates Foundation (OPP1109789) and from the National Natural Science Foundation of China (31570129) and start-up funds from Tsinghua University to BJ and from the Swedish Research Council (2018-05498, 2016-06264) and Cral-Tryggers Foundation (CTS 18:338) grants to SS. BJ is an Investigator of the Wellcome Trust (207487/B/17/Z).

Author Contributions

YXC and BJ designed the experiments and interpreted the data. YXC performed the majority of the experiments, with XG performing the biochemical experiments. ZYX and YXC analyzed the ribosome profile data. BWW and JHZ helped analyze the Tnseq data. ZJL, SS and BJ supervised research. YXC and BJ wrote the manuscript with input from the other authors.

Declaration of Interests

The authors declare no competing interests

References

Akanuma, G., Nanamiya, H., Natori, Y., Nomura, N., and Kawamura, F. (2006). Liberation of zinc-containing L31 (RpmE) from ribosomes by its paralogous gene product, YtiA, in Bacillus subtilis. J Bacteriol *188*, 2715-2720.

Baranowski, C., Welsh, M.A., Sham, L.T., Eskandarian, H.A., Lim, H.C., Kieser, K.J., Wagner, J.C., McKinney, J.D., Fantner, G.E., Ioerger, T.R.*, et al.* (2018). Maturing Mycobacterium smegmatis peptidoglycan requires non-canonical crosslinks to maintain shape. Elife *7*.

Becker, A.H., Oh, E., Weissman, J.S., Kramer, G., and Bukau, B. (2013). Selective ribosome profiling as a tool for studying the interaction of chaperones and targeting factors with nascent polypeptide chains and ribosomes. Nat Protoc *8*, 2212-2239.

Brenner, S., Jacob, F., and Meselson, M. (1961). An unstable intermediate carrying information from genes to ribosomes for protein synthesis. Nature *190*, 576-581.

Byrgazov, K., Vesper, O., and Moll, I. (2013). Ribosome heterogeneity: another level of complexity in bacterial translation regulation. Curr Opin Microbiol *16*, 133-139.

Chai, A.F., Bulloch, E.M., Evans, G.L., Lott, J.S., Baker, E.N., and Johnston, J.M. (2015). A covalent adduct of MbtN, an acyl-ACP dehydrogenase from Mycobacterium tuberculosis, reveals an unusual acyl-binding pocket. Acta Crystallogr D Biol Crystallogr *71*, 862-872.

Chaudhuri, S., Li, L., Zimmerman, M., Chen, Y., Chen, Y.X., Toosky, M.N., Gardner, M., Pan, M., Li, Y.Y., Kawaji, Q.*, et al.* (2018). Kasugamycin potentiates rifampicin and limits emergence of resistance in Mycobacterium tuberculosis by specifically decreasing mycobacterial mistranslation. Elife *7*.

Cortes, T., Schubert, O.T., Rose, G., Arnvig, K.B., Comas, I., Aebersold, R., and Young, D.B. (2013). Genome-wide mapping of transcriptional start sites defines an extensive leaderless transcriptome in Mycobacterium tuberculosis. Cell reports *5*, 1121-1131.

Crick, F.H. (1958). On protein synthesis. Symp Soc Exp Biol *12*, 138-163.

Culviner, P.H., and Laub, M.T. (2018). Global Analysis of the E. coli Toxin MazF Reveals Widespread Cleavage of mRNA and the Inhibition of rRNA Maturation and Ribosome Biogenesis. Mol Cell *70*, 868-880 e810.

DeJesus, M.A., Ambadipudi, C., Baker, R., Sassetti, C., and Ioerger, T.R. (2015). TRANSIT--A Software Tool for Himar1 TnSeq Analysis. PLoS Comput Biol *11*, e1004401.

Deusser, E., and Wittmann, H.G. (1972). Ribosomal proteins: variation of the protein composition in Escherichia coli ribosomes as function of growth rate. Nature *238*, 269-270.

Dinman, J.D. (2016). Pathways to Specialized Ribosomes: The Brussels Lecture. J Mol Biol *428*, 2186-2194.

Dow, A., and Prisic, S. (2018). Alternative ribosomal proteins are required for growth and morphogenesis of Mycobacterium smegmatis under zinc limiting conditions. PLoS One *13*, e0196300.

Elgamal, S., Katz, A., Hersch, S.J., Newsom, D., White, P., Navarre, W.W., and Ibba, M. (2014). EF-P dependent pauses integrate proximal and distal signals during translation. PLoS Genet *10*, e1004553.

Gaballa, A., Wang, T., Ye, R.W., and Helmann, J.D. (2002). Functional analysis of the Bacillus subtilis Zur regulon. J Bacteriol *184*, 6508-6514.

Gabriel, S.E., and Helmann, J.D. (2009). Contributions of Zur-controlled ribosomal proteins to growth under zinc starvation conditions. J Bacteriol *191*, 6116-6122.

Genuth, N.R., and Barna, M. (2018a). The Discovery of Ribosome Heterogeneity and Its Implications for Gene Regulation and Organismal Life. Mol Cell *71*, 364-374.

418 Genuth, N.R., and Barna, M. (2018b). Heterogeneity and specialized functions of translation
419 machinery: from genes to organisms. Nat Rev Genet *19*, 431-452.
420 Gerst, J.E. (2018). Pimp My Ribosome: Ribosomal Protein Paralogs Specify Translational Control.
421 Trends Genet *34*, 832-845.
422 Gohara, D.W., and Yap, M.F. (2018). Survival of the drowsiest: the hibernating 100S ribosome in
423 bacterial stress management. Curr Genet *64*, 753-760.
424 Hentschel, J., Burnside, C., Mignot, I., Leibundgut, M., Boehringer, D., and Ban, N. (2017). The
425 Complete Structure of the Mycobacterium smegmatis 70S Ribosome. Cell reports *20*, 149-160.
426 Ingolia, N.T., Brar, G.A., Rouskin, S., McGeachy, A.M., and Weissman, J.S. (2012). The ribosome
427 profiling strategy for monitoring translation in vivo by deep sequencing of ribosome-protected
428 mRNA fragments. Nat Protoc *7*, 1534-1550.
429 Jobe, A., Liu, Z., Gutierrez-Vargas, C., and Frank, J. (2019). New Insights into Ribosome Structure
430 and Function. Cold Spring Harb Perspect Biol *11*.
431 Kaberdina, A.C., Szaflarski, W., Nierhaus, K.H., and Moll, I. (2009). An unexpected type of
432 ribosomes induced by kasugamycin: a look into ancestral times of protein synthesis? Mol Cell *33*,
433 227-236.
434 Keren, I., Minami, S., Rubin, E., and Lewis, K. (2011). Characterization and transcriptome analysis
435 of Mycobacterium tuberculosis persisters. MBio *2*, e00100-00111.
436 Kieser, K.J., Baranowski, C., Chao, M.C., Long, J.E., Sassetti, C.M., Waldor, M.K., Sacchettini, J.C.,
437 Ioerger, T.R., and Rubin, E.J. (2015). Peptidoglycan synthesis in Mycobacterium tuberculosis is
438 organized into networks with varying drug susceptibility. Proc Natl Acad Sci U S A *112*, 13087-
439 13092.
440 Kondrashov, N., Pusic, A., Stumpf, C.R., Shimizu, K., Hsieh, A.C., Ishijima, J., Shiroishi, T., and
441 Barna, M. (2011). Ribosome-mediated specificity in Hox mRNA translation and vertebrate tissue
442 patterning. Cell *145*, 383-397.
443 Koripella, R.K., Holm, M., Dourado, D., Mandava, C.S., Flores, S., and Sanyal, S. (2015). A
444 conserved histidine in switch-II of EF-G moderates release of inorganic phosphate. Sci Rep *5*,
445 12970.
446 Kurylo, C.M., Parks, M.M., Juette, M.F., Zinshteyn, B., Altman, R.B., Thibado, J.K., Vincent, C.T.,
447 and Blanchard, S.C. (2018). Endogenous rRNA Sequence Variation Can Regulate Stress Response
448 Gene Expression and Phenotype. Cell reports *25*, 236-248 e236.
449 Lange, C., Lehr, M., Zerulla, K., Ludwig, P., Schweitzer, J., Polen, T., Wendisch, V.F., and Soppa, J.
450 (2017). Effects of Kasugamycin on the Translatome of Escherichia coli. PLoS One *12*, e0168143.
451 Langmead, B., and Salzberg, S.L. (2012). Fast gapped-read alignment with Bowtie 2. Nat
452 Methods *9*, 357-359.
453 Li, G.W., Oh, E., and Weissman, J.S. (2012). The anti-Shine-Dalgarno sequence drives
454 translational pausing and codon choice in bacteria. Nature *484*, 538-541.
455 Li, Y., Sharma, M.R., Koripella, R.K., Wade, J.T., Gray, T.A., Derbyshire, K.M., Agrawal, R.K., and
456 Ojha, A.K. (2019). Reply to Tobiasson et al.: Zinc depletion is a specific signal for induction of
457 ribosome hibernation in mycobacteria. Proc Natl Acad Sci U S A.
458 Li, Y., Sharma, M.R., Koripella, R.K., Yang, Y., Kaushal, P.S., Lin, Q., Wade, J.T., Gray, T.A.,
459 Derbyshire, K.M., Agrawal, R.K., *et al.* (2018a). Zinc depletion induces ribosome hibernation in
460 mycobacteria. Proc Natl Acad Sci U S A *115*, 8191-8196.
461 Li, Z., Ge, X., Zhang, Y., Zheng, L., Sanyal, S., and Gao, N. (2018b). Cryo-EM structure of
462 Mycobacterium smegmatis ribosome reveals two unidentified ribosomal proteins close to the
463 functional centers. Protein Cell *9*, 384-388.

464 Loayza-Puch, F., Rooijers, K., Buil, L.C., Zijlstra, J., Oude Vrielink, J.F., Lopes, R., Ugalde, A.P., van
465 Breugel, P., Hofland, I., Wesseling, J., *et al.* (2016). Tumour-specific proline vulnerability
466 uncovered by differential ribosome codon reading. Nature *530*, 490-494.
467 Madigan, C.A., Martinot, A.J., Wei, J.R., Madduri, A., Cheng, T.Y., Young, D.C., Layre, E., Murry,
468 J.P., Rubin, E.J., and Moody, D.B. (2015). Lipidomic analysis links mycobactin synthase K to iron
469 uptake and virulence in M. tuberculosis. PLoS pathogens *11*, e1004792.
470 Makarova, K.S., Ponomarev, V.A., and Koonin, E.V. (2001). Two C or not two C: recurrent
471 disruption of Zn-ribbons, gene duplication, lineage-specific gene loss, and horizontal gene
472 transfer in evolution of bacterial ribosomal proteins. Genome Biol *2*, RESEARCH 0033.
473 Mandava, C.S., Peisker, K., Ederth, J., Kumar, R., Ge, X., Szaflarski, W., and Sanyal, S. (2012).
474 Bacterial ribosome requires multiple L12 dimers for efficient initiation and elongation of protein
475 synthesis involving IF2 and EF-G. Nucleic Acids Res *40*, 2054-2064.
476 Marzi, S., Myasnikov, A.G., Serganov, A., Ehresmann, C., Romby, P., Yusupov, M., and Klaholz,
477 B.P. (2007). Structured mRNAs regulate translation initiation by binding to the platform of the
478 ribosome. Cell *130*, 1019-1031.
479 Mets, T., Kasvandik, S., Saarma, M., Maivali, U., Tenson, T., and Kaldalu, N. (2019).
480 Fragmentation of Escherichia coli mRNA by MazF and MqsR. Biochimie *156*, 79-91.
481 Mohammad, F., Woolstenhulme, C.J., Green, R., and Buskirk, A.R. (2016). Clarifying the
482 Translational Pausing Landscape in Bacteria by Ribosome Profiling. Cell reports *14*, 686-694.
483 Moore, P.B., Traut, R.R., Noller, H., Pearson, P., and Delius, H. (1968). Ribosomal proteins of
484 Escherichia coli. II. Proteins from the 30 s subunit. J Mol Biol *31*, 441-461.
485 Murphy, K.C., Papavinasasundaram, K., and Sassetti, C.M. (2015). Mycobacterial recombineering.
486 Methods in molecular biology *1285*, 177-199.
487 Nakamura, Y., Gojobori, T., and Ikemura, T. (2000). Codon usage tabulated from international
488 DNA sequence databases: status for the year 2000. Nucleic Acids Res *28*, 292.
489 Nanamiya, H., Akanuma, G., Natori, Y., Murayama, R., Kosono, S., Kudo, T., Kobayashi, K.,
490 Ogasawara, N., Park, S.M., Ochi, K., *et al.* (2004). Zinc is a key factor in controlling alternation of
491 two types of L31 protein in the Bacillus subtilis ribosome. Mol Microbiol *52*, 273-283.
492 Nedialkova, D.D., and Leidel, S.A. (2015). Optimization of Codon Translation Rates via tRNA
493 Modifications Maintains Proteome Integrity. Cell *161*, 1606-1618.
494 Novoa, E.M., and Ribas de Pouplana, L. (2012). Speeding with control: codon usage, tRNAs, and
495 ribosomes. Trends Genet *28*, 574-581.
496 Oh, E., Becker, A.H., Sandikci, A., Huber, D., Chaba, R., Gloge, F., Nichols, R.J., Typas, A., Gross,
497 C.A., Kramer, G., *et al.* (2011). Selective ribosome profiling reveals the cotranslational chaperone
498 action of trigger factor in vivo. Cell *147*, 1295-1308.
499 Parenteau, J., Lavoie, M., Catala, M., Malik-Ghulam, M., Gagnon, J., and Abou Elela, S. (2015).
500 Preservation of Gene Duplication Increases the Regulatory Spectrum of Ribosomal Protein
501 Genes and Enhances Growth under Stress. Cell reports *13*, 2516-2526.
502 Prisic, S., Hwang, H., Dow, A., Barnaby, O., Pan, T.S., Lonzanida, J.A., Chazin, W.J., Steen, H., and
503 Husson, R.N. (2015). Zinc regulates a switch between primary and alternative S18 ribosomal
504 proteins in Mycobacterium tuberculosis. Mol Microbiol *97*, 263-280.
505 Ramakrishnan, V. (2014). The ribosome emerges from a black box. Cell *159*, 979-984.
506 Robinson, M.D., McCarthy, D.J., and Smyth, G.K. (2010). edgeR: a Bioconductor package for
507 differential expression analysis of digital gene expression data. Bioinformatics *26*, 139-140.
508 Rodnina, M.V. (2018). Translation in Prokaryotes. Cold Spring Harb Perspect Biol *10*.
509 Sassetti, C.M., Boyd, D.H., and Rubin, E.J. (2001). Comprehensive identification of conditionally
510 essential genes in mycobacteria. Proc Natl Acad Sci U S A *98*, 12712-12717.

511 Sawyer, E.B., Grabowska, A.D., and Cortes, T. (2018). Translational regulation in mycobacteria
512 and its implications for pathogenicity. Nucleic Acids Res *46*, 6950-6961.
513 Schuller, A.P., Wu, C.C., Dever, T.E., Buskirk, A.R., and Green, R. (2017). eIF5A Functions Globally
514 in Translation Elongation and Termination. Mol Cell *66*, 194-205 e195.
515 Segev, N., and Gerst, J.E. (2018). Specialized ribosomes and specific ribosomal protein paralogs
516 control translation of mitochondrial proteins. J Cell Biol *217*, 117-126.
517 Shell, S.S., Wang, J., Lapierre, P., Mir, M., Chase, M.R., Pyle, M.M., Gawande, R., Ahmad, R.,
518 Sarracino, D.A., Ioerger, T.R.*, et al.* (2015). Leaderless Transcripts and Small Proteins Are
519 Common Features of the Mycobacterial Translational Landscape. PLoS Genet *11*, e1005641.
520 Shi, Z., Fujii, K., Kovary, K.M., Genuth, N.R., Rost, H.L., Teruel, M.N., and Barna, M. (2017).
521 Heterogeneous Ribosomes Preferentially Translate Distinct Subpools of mRNAs Genome-wide.
522 Mol Cell *67*, 71-83 e77.
523 Siegrist, M.S., Unnikrishnan, M., McConnell, M.J., Borowsky, M., Cheng, T.Y., Siddiqi, N., Fortune,
524 S.M., Moody, D.B., and Rubin, E.J. (2009). Mycobacterial Esx-3 is required for mycobactin-
525 mediated iron acquisition. Proc Natl Acad Sci U S A *106*, 18792-18797.
526 Snapper, S.B., Melton, R.E., Mustafa, S., Kieser, T., and Jacobs, W.R., Jr. (1990). Isolation and
527 characterization of efficient plasmid transformation mutants of Mycobacterium smegmatis. Mol
528 Microbiol *4*, 1911-1919.
529 Song, W., Joo, M., Yeom, J.H., Shin, E., Lee, M., Choi, H.K., Hwang, J., Kim, Y.I., Seo, R., Lee, J.E.,
530 *et al.* (2019). Divergent rRNAs as regulators of gene expression at the ribosome level. Nat
531 Microbiol *4*, 515-526.
532 Su, H.W., Zhu, J.H., Li, H., Cai, R.J., Ealand, C., Wang, X., Chen, Y.X., Kayani, M.U., Zhu, T.F.,
533 Moradigaravand, D.*, et al.* (2016). The essential mycobacterial amidotransferase GatCAB is a
534 modulator of specific translational fidelity. Nat Microbiol *1*, 16147.
535 Tobiasson, V., Dow, A., Prisic, S., and Amunts, A. (2019). Zinc depletion does not necessarily
536 induce ribosome hibernation in mycobacteria. Proc Natl Acad Sci U S A.
537 Trauner, A., Lougheed, K.E., Bennett, M.H., Hingley-Wilson, S.M., and Williams, H.D. (2012). The
538 dormancy regulator DosR controls ribosome stability in hypoxic mycobacteria. J Biol Chem *287*,
539 24053-24063.
540 van de Waterbeemd, M., Fort, K.L., Boll, D., Reinhardt-Szyba, M., Routh, A., Makarov, A., and
541 Heck, A.J. (2017). High-fidelity mass analysis unveils heterogeneity in intact ribosomal particles.
542 Nat Methods *14*, 283-286.
543 Vesper, O., Amitai, S., Belitsky, M., Byrgazov, K., Kaberdina, A.C., Engelberg-Kulka, H., and Moll, I.
544 (2011). Selective translation of leaderless mRNAs by specialized ribosomes generated by MazF in
545 Escherichia coli. Cell *147*, 147-157.
546 Warren, A.J. (2018). Molecular basis of the human ribosomopathy Shwachman-Diamond
547 syndrome. Adv Biol Regul *67*, 109-127.
548 Yang, K., Chang, J.Y., Cui, Z., Li, X., Meng, R., Duan, L., Thongchol, J., Jakana, J., Huwe, C.M.,
549 Sacchettini, J.C.*, et al.* (2017). Structural insights into species-specific features of the ribosome
550 from the human pathogen Mycobacterium tuberculosis. Nucleic Acids Res *45*, 10884-10894.
551 Yutin, N., Puigbo, P., Koonin, E.V., and Wolf, Y.I. (2012). Phylogenomics of prokaryotic ribosomal
552 proteins. PLoS One *7*, e36972.
553 Zhang, Y., Duc, A.C., Rao, S., Sun, X.L., Bilbee, A.N., Rhodes, M., Li, Q., Kappes, D.J., Rhodes, J.,
554 and Wiest, D.L. (2013). Control of hematopoietic stem cell emergence by antagonistic functions
555 of ribosomal protein paralogs. Dev Cell *24*, 411-425.

556

557

Figure Legends

Figure 1. Alternative mycobacterial ribosomes engage in gene translation. (A) Sequence alignments of AltRpsR and CanRpsR in 4 mycobacterial species (top and middle panels) and the AltRpSR and CanRpsR from *M. smegmatis* (bottom panel). (B) Cartoon representing the C-terminus affinity tagging of the native CanRpsR and AltRpsR native loci. (C) Anti-FLAG and anti-HA Western blots of cell lysate (top panel) and of ribosome pellets (bottom panel) in complete 7H9 medium (7H9) and in standard Sauton's medium (Sauton) or Sauton's medium supplemented with zinc sulfate (at indicated concentrations). (D) Polysomes were isolated and subjected to +/- MNase digestion (cartoon). Following digestion, AltRibos were isolated by FLAG-immunoprecipitation and the fraction blotted with anti-FLAG and anti-HA antibodies. Relative quantification by image analysis of AltRpsR and CanRpsR with our without digestion from the western blots is shown in the histogram. (E) Di-peptide formation of AltRibos vs CabRibos with a fully reconstituted mycobacterial translation system (Li et al., 2018b). Peptides were detected and analyzed by high performance liquid chromatography (HPLC).

Figure 2. Alternative ribosomes have distinct translational profiles. (A) Cartoon outlining work-flow for performing selective ribosome profiling in the two RpsR-tagged strains – strain A and strain B (and see Methods). (B) Western blot against FLAG (AltRibo) and HA (CanRibo) following isolation of ribosomes for ribosome profiling as in (A). Blots from two biological replicates are shown. (C) Scatter plot showing selective ribosome profiles compared with total ribosome input in Strain A and Strain B. Axes represent reads per kilobase per million mapped reads (RPKM). Blue and red dots represent down- and up-regulated reads respectively (and see Fig. 5A). R^2 represents Pearson correlation. (D) Correlation of translation efficiency of total ribosome, selective CanRibo and selective AltRibo inputs in Strain A compared with Strain B. R^2 represents Pearson correlation.

Figure 3. Alternative ribosomes have 5' read accumulation compared with canonical ribosomes. (A) Normalized reads of each ribosome input for the gene *Msmeg_0363* were plotted along gene length using IGV software (see Methods). Reads from AltRibos show a clear 5' accumulation compared with reads generated from CanRibos or total ribosomal input. (B) Shifts in polarity scores for the entire genome generated from selective AltRibo and CanRibo reads from Strains A and B – blue dots represent shifts calculated from AltRibos and gray squares represent shifts calculated from CanRibos. The overall polarity score shifts are illustrated as smoothed curves above and to the right of the plot. A negative score indicates 5' read accumulation and a positive score indicates a 3' read accumulation.

Figure 4. Alternative ribosomes have distinct codon preferences compared with canonical ribosomes. The relative A-site codon occupancy for all 61 sense codons for AltRibos and CanRibos in Strain A (A) and Strain B (B) compared with total ribosome input. Cumulative probability and violin (inset) plots for correlation between codon occupancy for AltRibos and CanRibos compared with total ribosome input from both Strain A (C) and Strain B (D). *** $p<0.001$ by Student's t-test. (E) Combining data from Strain A and B, AltRibos have 12 high and 12 low occupancy codons compared with CanRibos. (F) The relative codon frequencies of the 5' 50 codons and 3' 50 codons for each ORF were analyzed. Comparing AltRibo high occupancy codons (left panel) and low occupancy codons (right panel – both from E above) with non-significantly enriched codons, there was significant enrichment of high occupancy codons at the beginning of ORFs, and a trend towards enrichment of low occupancy codons at the end of ORFs by chi-squared test. (G) The extent of initiation complex formation by AltRibos compared with CanRibos measured by retention of ^{3}H-fMet count on a nitrocellulose filter (see Methods). (H) The kinetics and extent of binding of the initiator tRNA to the mRNA programmed 70S ribosome (AltRibo vs CanRibo) followed with BODIPY fluorescence

Figure 5. Alternative ribosomes have translational bias for a subset of genes. Normalized ribosome profile read density for CanRibos (A) and AltRibos (B) compared with total ribosome input in Strain A (left panel) and Strain B (right panel). Significantly upregulated ($\log_2$ fold-change (FC) >0.5, p-value <0.05) and downregulated ($\log_2$ FC<0.5, p-value <0.05) genes are represented by red and blue dots respectively. Degree of overlap in up- and down-regulated genes in the two strains are shown by Venn diagrams (C). (D) Heatmap of the 209 up- and 522 down-regulated genes by AltRibos, clustered by relative translation efficiency by ribosome profiling from each biological replicate for AltRibos compared with total ribosome input across both strains A and B. (E) Gene ontology analysis (using DavidTools) of the top three low-enriched translated genes from AltRibos.

Figure 6. Synthetic lethal interaction analysis reveals a role for the AltRP operon in iron homeostasis. (A) Western blot against CanRpsR (anti-HA) and AltRpsR (anti-FLAG) for wild-type *M. smegmatis* scraped from 7H10-agar plates supplemented with increasing concentrations of TPEN. Antibody against EF-Tu was used as a loading control. (B) Upper panel: Volcano plot of fold-change in transposon insertions against p-value by resampling test for Tnseq analysis of wild-type *M. smegmatis* plated without zinc depletion (WT) versus wild-type *M. smegmatis* plated on 7H10-agar supplemented with TPEN (WT+TPEN). Significantly over- and under-represented transposon insertions (p-value <0.05, $\log_2$ FC >1 or $\log_2$ FC <-1 by resampling test) are shown in red and blue respectively. Lower panel: Transposon insertion reads in wild-type *M. smegmatis* plated without zinc depletion (WT) and on 7H10-agar + TPEN (WT+TPEN) for the TA loci in the four AltRP genes. Number of normalized transposon reads per TA locus are shown above the bar graphs. (C) Volcano plots as in (B) for Tnseq analysis comparing wild-type *M. smegmatis* or *M. smegmatis*-ΔAltRP (ΔAltRP) plated without zinc depletion or on 7H10+TPEN ("+TPEN"). (D) Transposon insertion reads in wild-type *M. smegmatis* or *M. smegmatis*-ΔAltRP (ΔAltRP) plated without zinc depletion and on 7H10-agar + TPEN ("+TPEN") for the TA loci in

the gene coding for MbtN. Number of normalized transposon reads per TA locus are shown above the bar graphs. (E) Growth curve (as measured by OD_{600nm}) in chelated medium for wild-type *M. smegmatis*, *M. smegmatis*-ΔAltRP (ΔAltRP), *M. smegmatis*-ΔAltRP complemented with the AltRP operon (ΔAltRP + AltRP), or *M. smegmatis*-ΔAltRP (ΔAltRP) grown in chelated medium subsequently supplemented with iron (ΔAltRP + 10μM $FeCl_3$) or zinc (ΔAltRP + 10μM $ZnSO_4$). Data show biological triplicates +/- SD and results are representative of two independent experiments. * $p<0.05$, ** $p<0.01$, *** $p<0.001$ by Student's t-test. Brown asterisks represent comparison between ΔAltRP and ΔAltRP+10μM $FeCl_3$, green asterisks represent comparison between ΔAltRP and ΔAltRP+10μM $ZnSO_4$.

Supplementary Figure Legends

Figure S1. (A) Growth curves (as measured by OD_{600nm}) for wild-type *M. smegmatis*, *M. smegmatis*-ΔAltRP (ΔAltRP) and *M. smegmatis*-ΔAltRP::AltRP (ΔAltRP+AltRP) in zinc-replete complete 7H9 medium (left panel) and relatively zinc-deplete Sauton's medium (right panel). Three biological replicates +/- SD are plotted (B) Cartoon representing the work-flow for immunoprecipitation of FLAG-tagged AltRpsR (left panel) and total ribosomes (right panel). (C) Coomassie-stained SDS-PAGE gels of anti-FLAG eluate and 70S ribosomes from sucrose-density centrifugation as shown in (B).

Figure S2. (A) Anti-FLAG (CanRpsR) and anti-HA (AltRpsR) Western blots of Strain B cell lysate in complete 7H9 medium (7H9) and in standard Sauton's medium (Sauton) or Sauton's medium supplemented with zinc sulfate (at indicated concentrations). (B) Pearson correlation analysis of selective AltRibo, CanRibo and total ribosome profiles of the two biological replicates from each strain used in this study.

Figure S3. Ribosome profile reads show clear 3 nucleotide periodicity. Representative ribosome profile 28nt reads from each replicate from Strains A (A) and B (B) used in this analysis.

Figure S4. Pearson correlation analysis of paired RNAseq of the two biological replicates from each strain used in this study.

Figure S5. Gene ontology analysis of enriched AltRibo translated genes. Analysis as per Fig. 5E. The top three enriched hits are shown (Strain A had only two statistically significant enriched hits).

STAR METHODS

KEY RESOURCES TABLE

See separate attached file.

CONTACT FOR REAGENT AND RESOURCES SHARING

Further information and requests for reagents may be directed to, and will be fulfilled by the lead contact (BJ).

METHOD DETAILS

Bacterial strains and culture

Wild-type *M. smegmatis* mc^2-155 (Snapper et al., 1990) and derived strains were grown in either Middlebrook 7H9 media supplemented with 0.2% glycerol, 0.05% Tween-80, 10% ADS (albumin-dextrose-salt) with appropriate antibiotics or Sauton's medium (0.05% KH_2PO_4, 0.05% $MgSO_4 \cdot 7H_2O$, 0.2% citric acid, 0.005% ferric ammonium citrate, 6% glycerol, 0.4% asparagine, 0.05% Tween, pH 7.4) (Prisic et al., 2015). Zinc sulfate at indicated concentrations was added to Sauton medium as per specific protocols. For the iron depletion experiments, we modified a previous method (Siegrist et al., 2009). Briefly, Sauton's medium was prepared as above with the exception of the magnesium sulfate, but after preparation, 10g of chelex 100 resin was added to 1L of medium, thoroughly mixed, and left for 24 hrs. The medium was sterile-filtered to remove the chelating agent beads, and 1g sterile $MgSO_4 \cdot 7H_2O$ added to the medium. Zinc sulfate and iron chloride were also supplemented at the indicated concentrations as appropriate for the experimental condition. If not otherwise noted, bacteria were grown and maintained at 37°C with shaking.

M. smegmatis AltRP KO strain and complemented strain construction

In normal conditions (High Zinc), the AltRP operon is not required for growth. A double crossover strategy was used to construct an unmarked AltRP knockout strain as previously described (Su et al., 2016). Sequences 1,000bp upstream and downstream of the operon were cloned and ligated into the P2NIL suicide vector. The lacZ and SacB gene were cloned from pGOAL17 and ligated to P2NIL containing upstream and downstream 1,000bp region to generate the AltRP deletion construct. 2μg plasmid were transformed to wild-type *M. smegmatis* competent cells by electrophoresis and selected on LB plates supplemented with 25μg/ml kanamycin and 50μg/ml X-gal. Blue colonies were screened for single crossover recombinants and further verified by PCR. Correctly identified recombinants were further plated on LB plates containing X-gal and 2% sucrose with ten-fold serial dilutions. White colonies were screened for double crossover strains by PCR verification. A correct knock-out strain was further verified by Southern blot and used in subsequent experiments.

For complementation of the knock-out strain, the upstream 500bp of the coding region for the AltRP operon (presumably incorporating the promoter region) along with the whole AltRP operon was cloned with C-terminal 3xFlag tag to AltRpsR and ligated to pML1342 as a complementation plasmid. The plasmid was transformed to ΔAltRP competent cells and plated on LB plates with 50μg/ml hygromycin. Recombinants were further verified by western blot in Sauton medium supplemented with different concentrations of zinc to check the expression from the operon.

Generating endogenous AltRpsR/CanRpsR with different affinity tags strains

Upstream 500bp (US500) and downstream 500bp (DS500) of AltRpsR/CanRpsR stop codons were cloned. Different affinity tag sequences (3xFlag/3xHA) fused with different antibiotic expression cassette (Hygromycin/Zeocin) were generated by overlap PCR (3xFlag-Zeo oligo cassette was kindly provided by JHZ). The upstream, tag-antibiotic, downstream cassette were

fused by Gibson assembly and cloned into pUC19 vector. pUC19 plasmid containing four different recombineering oligo cassette (AltRpsR-3Flag-Zeo, AltRpsR-3HA-Hyg, CanRpsR-3HA-Hyg and CanRpsR-3Flag-Zeo) were generated. *M. smegmatis* containing the plasmid pNitET-SacB-kan (Murphy et al., 2015) was grown to OD_{600nm}≈0.2 and 10μM isovaleronitril (IVN) was added to induce the expression of RecET, after inducing for 6h, competent cells were prepared by 3 washes in 10% glycerol. Oligos for recombineering were amplified from pUC19 series plasmid and 2μg DNA were transformed to the competent cells. Bacteria were plated on LB plates supplemented with either 50μg/ml hygromycin or 20μg/ml zeocin. Desired colonies were genotyped by PCR and further verified by Western Blot to test the expression of AltRpsR/CanRpsR by blotting against with either Flag or HA antibody.

Western Blot to test zinc-switch phenotype

Strain A and Strain *B* were cultured in 7H9 medium to stationary phase (OD_{600nm}≈3) and sub-cultured 1:500 to Sauton medium (zinc-free) supplemented with different concentrations of zinc sulfate. When bacteria reached stationary phase, bacteria were washed and re-suspended in TE buffer. The bacterial suspension was disrupted by beads-beating and lysate centrifuged at 17,950x*g*, 4°C for 5 min. Protein concentration was quantified by Bradford assay (Bio-rad) and same amount of protein were loaded onto 5%/12% SDS-PAGE gel. Proteins were further transferred onto PVDF membrane (Bio-rad). The membrane was blocked in 4% skim milk at room temperature (RT) for 1 h. Primary antibody was diluted 1:2000 and the blot was incubated at 4°C overnight. The membrane was then washed with TBS-T at RT and secondary antibody, diluted, 1:5000 rate and incubated at RT for 1 h. After washing with TBS-T, the image was developed by ECL Western Blotting Substrate (Pierce).

70S ribosome purification of *M. smegmatis*

M. smegmatis AltRP knockout strain was grown on Middlebrook 7H9 medium till OD_{600nm}≈1 and collected by centrifuge at 4500x*g*, 4°C for 20 min. The bacterial pellet was washed and re-suspended with polysome buffer (50mM Tris-actate pH=7.2, 12mM $MgCl_2$, 50mM NH_4Cl). Bacteria were pulverized by French-press, and the lysate were centrifuged at 18500x*g*, 4°C for 45 min. Cleared lysate were further loaded to a linear sucrose gradient (10%-50%) at Beckman SW41 rotor and centrifuged at 39,000 rpm, 4°C for 5 h. Gradients were fractioned with continuous A_{260} measurement and the corresponding 70S peak was collected for downstream analysis.

Selective ribosome profiling with affinity- purified tagged AltRibosomes

Bacterial cultures of dual-tagged Strain A or Strain B were grown till $OD600_{nm}$≈1 and treated with 100μg/ml chloramphenicol for 3 mins to arrest elongating ribosome before harvesting bacteria. Bacterial pellet were collect by centrifuging at 4500x*g*, 4°C for 10 min. The pellet were washed and re-suspended with ice-cold polysome buffer with minor recipe change. (50mM Tris-actate pH= 7.2, 12mM MgCl2, 50mM NH_4Cl, 10mM CaCl2 and 100μg/ml chloramphenicol) The suspended bacterial suspension was dropped into liquid nitrogen and smashed into powder. The powder was smashed several times with repeatedly chilling with liquid nitrogen and was further pulverized with beads beating 4 to 5 times with chilling in liquid nitrogen between each step. After centrifugation at 18500x*g* for 45 min, the cleared lysate was transferred to a new tube supplied with 70U/ml MNase to digest ribosome-unprotected mRNA. The pre-digested lysate was laid over a 1M sucrose cushion and centrifuged at 30,000 rpm, 4°C for 20 h in Beckman 70Ti rotor. After ultracentrifugation, the ribosome pellet was washed and dissolved in polysome buffer. The dissolved ribosome solution was further digested with MNase at 4°C for 1 h. The digested ribosome fraction was incubated with either Flag resin or HA resin at 4°C overnight. After washing of the bound resin, the resin was eluted with 3xFlag/3xHA peptide to isolate the

AltRibo (eluate), and the remaining flow-through was confirmed as consisting almost entirely of CanRibos.

The procedure for building deep sequencing libraries was followed as previously described (Ingolia et al., 2012) with minor changes. The detailed protocol is described as below. Ribosome-protected mRNA fragments were extracted by miRNeasy kit according to the manufacturer's instructions and size-selected for 26-34nt fragment by marker oligo through 15% TBE-UREA PAGE. The corresponding region was sliced and smashed into pieces and soaked in 400μl RNA gel extraction buffer (300mM sodium acetate pH 5.5, 1mM EDTA and 0.25% SDS) and rotated at room temperature overnight. RNA was precipitated with 1.5μl GlycoBlue and 500μl isopropanol. The RNA was dephosphorylated with 1μl T4 PNK at 37°C for 1 h. RNA was extracted by isopropanol precipitation. Samples were then ligated with 0.5μl Universal miRNA cloning linker and 1.0μl T4 RNA ligase (truncated) at room tempreate overnight. The ligation production was purified by isopropanol precipitation and visulized by 15% TBE-UREA PAGE. After slicing the corresponding ligated mRNA fragment, the samples were then subjected to reverse transcription with supersciptase III and RT-Primer. After incubating the reaction at 48°C, 30 min, the RNA template was further hydrolyzed with 2μl 1M NaOH at 98°C for 20 min. The RT product was precipitated with isopropanol and size-selcted with 15% TBE-UREA PAGE. The corresponding region was sliced and soaked in 400μl DNA gel extraction (300mM NaCl, 10mM Tris pH=8, and 1mM EDTA) and rotated at RT overnight. The cDNA was purified by isopropanol precipitation and circularized with 1μl CircLigase and incubated at 80°C for 1 h. The circularized cDNA template was incubated with 1μl 10mM Biotinylated rRNA subtraction oligo pool mix. The Oligo sequence was the same as from another study (Shell et al., 2015) with additional oligos newly designed according to our preliminary ribo-seq data (Table S2). The mixture was denatured for 90s at 100°C and then anneal at 0.1°C /sec to 37°C. This was then incubated at 37°C for 15 min. 30μl streptavidin C1 DynaBeads was added to the mixture and

incubated for 15 min at 37°C with mixing at 1000 rpm. Then the mixture was placed on a magnetic rack to isolate the beads, the supernatant was transferred to a new tube and purifed by isopropanol precipitation. The subsequent cDNA template was used for library amplification with Phusion high-fidelity DNA polyermase for 12-14 cycles. PCR products were purifed from 8% TBE PAGE gel. The corresponding bands were sliced and soaked in DNA gel extraction buffer and rotated at room temperature overnight. The PCR products were purified by isopropanol precipitation and the concentration and quality were measured with Agilent 2100 Bioanalyzer. Libraires were sequenced on the illumina X-ten sequencer.

Large-scale tagged ribosome purification for biochemical analysis

Bacterial cultures (~30L) were grown to around OD_{600nm}≈1 and bacterial pellets were collected by 4500x*g*, 20 min, 4°C. Pellet was washed and re-suspended in polysome buffer. Bacteria were disrupted by French Press and centrifuged at 18500x*g*, 4°C for 1h to collect supernatant. MNase was added to the cleared lysate at a concentration of 70U/ml and digested at 4°C overnight. The digested lysate was loaded onto 1M sucrose cushions and centrifuged at 30,000 rpm, 4°C for 20 h. After centrifugation, the supernatant was discarded, and the ribosome pellet washed with polysome buffer and dissolve in polysome buffer with gentle shaking at 4°C. The crude ribosome suspension was further digested with MNase at 4°C overnight. After secondary digestion, the ribosome preparation was dialyzed against HEPES-polymix buffer (Koripella et al., 2015; Mandava et al., 2012). The ribosome preparation was incubated with anti-Flag M2 beads 4°C overnight. After binding with M2 beads, the flow-through was collected as CanRibo and AltRibo was collected by eluting with Flag peptide. Each fraction, comprising total Ribo, CanRibo (flow through) and AltRibo (Eluate), were probed by Western blotting for quality check and purity prior to further analysis.

***In vitro* 70S initiation complex formation**

Initiation complex was formed by incubating 70S ribosome variants as described above (0.2 μM), [^{3}H]fMet-tRNA^{fMet} (0.5 μM), XR7mRNA (AUG-UAA) (0.5 μM), initiation factors (0.5 μM) and GTP (1 mM) at 37°C for 15 min in HEPES-polymix buffer (Koripella et al., 2015). The reactions were thereafter filtered through BA-85 nitrocellulose membranes and washed with 10ml of ice-cold HEPES-polymix buffer (pH 7.5). The radioactivity retained on the filter was measured in a Beckman LC6500 scintillation counter.

In vitro initiator tRNA binding

BODIPY labelled Met-tRNA^{fMet} (0.1 μM) was rapidly mixed in stopped flow with 70S ribosomes (1 μM) pre-incubated with XR7mRNA (AUG-UAA) (0.5 μM). BODIPY fluorescence was excited at 575 nm and the change in fluorescence signal was monitored in real time after passing through a 590 nm cut-off filter. The time course data was obtained by averaging 3-5 individual traces and fitted with single exponential model.

In vitro di-peptide assay

For Met-Leu dipeptide formation, an initiation complex was formed with mycobacterial 70S ribosome variants (1-5 μM), AUG-CUG-UAA XR7 mRNA (20 μM) and [^{3}H]fMet-tRNA^{fMet} (1 μM), initiation factors (2 μM) at 37°C. In parallel, an elongation mix was prepared which contained *M. smegmatis* EF-Tu (20 μM), EF-Ts (20 μM), tRNA^{Leu} (100 μM), Leu amino acid (0.5 mM), Leu-tRNA synthetase (1unit/μL) and GTP (1mM) at 37°C. Both initiation complex and elongation mix containing energy pump ATP (1mM), EP (10 mM), PK and MK (Sigma). The reaction was started by mixing equal volumes of the initiation complex and elongation complex at 37°C and was quenched after 10 s by adding 17% formic acid. The peptides were isolated from the ribosome complex by KOH treatment and further analyzed by HPLC equipped with a radioactivity detector.

Read preparation and alignment

The *M. smegmatis* mc^2-155 reference genome assembly (ASM1500v1) downloaded from Ensembl Bacteria Release 32 (https://bacteria.ensembl.org/) was used for all analyses. For RNAseq, we performed quality control and trimmed adaptors using the FastQC and FASTX-Toolkit. For ribosome profiling, after quality control and adaptor removal, reads less than 25nt long were discarded and longer than 36nt were trimmed to 36nt. Next, ribosome profile and RNAseq reads that aligned to rRNA and tRNA were removed using bowtie2 (Langmead and Salzberg, 2012). We aligned the remaining reads to the genome using bowtie2 with "sensitive-local" option. The mapped reads were normalized to reads per kilobase million (RPKM) using total number of mapped reads.

A-site assignment

For each read, the A-site's position was inferred by taking the first nucleotide that was 12nt upstream of the 3'end of the read (Mohammad et al., 2016). Based on this, we generated a signal track of A-sites for all transcripts. ORFs that had been annotated in the reference were denoted as annotated ORFs (aORFs).

Polarization of aligned Ribosome Profile reads

The polarity score was calculated on the basis of aligned A-site signal track by adapting a previous method (Schuller et al., 2017). To avioid ambigous artifacts that might be caused by peaks around the start/stop codons, we excluded the first and last 15nt of the coding region in the analysis. aORFs with more than 50 reads in coding sequences were plotted. In this study, we calculated the polarity score under AltRibo, CanRibo as well as total ribosomes population. Here we defined the concept of polarity shift by taking total ribosomes as the background input and substrating the polarity score of background from the score of AltRibo-enriched/CanRibo-enriched populations.

Differential ribosome codon reading

The calculation of codon occupancy was adaped from a previous method (Loayza-Puch et al., 2016). For each aORF, only in-frame ribosome profiling fragments (RPFs) were included to study the frequencies of all codons. For each coding gene, its codon density was calculated by normalizing the observed RPF frequencies by the total frequcies of codons. Later we included genes with at least 100 RPFs as input and obtained an averaged codon density for each codon. Here we denoted T_{codon_i} as the averaged codon occupancy of codon_i for AltRibo or CanRibo population while R_{codon_i} as the averaged codon occupancy of codon_i for reference population, in this case, the total ribosomes. To better clarify the difference between AltRibo and CanRibo population, we further defined codon occupancy shift as follows:

$$\mathrm{codon\ occupancy\ shift}_{\mathrm{codon}_i} = \left(T_{\mathrm{codon}_i} - R_{\mathrm{codon}_i}\right)/R_{\mathrm{codon}_i}.$$

Significantly different codon usage were detected by comparing the codon density of all studied aORFs under test conditions (AltRibo/CanRibo) against the corresponding density under the reference condition (total ribosome input) (t-test *p value* <0.05 and shift > 0.05 or shift < -0.05). Additionaly, for each individual aORF we correlated its codon density from AltRibo/CanRibo population with that from total ribosome population (Pearson correlation was used in this study).

Differential codon abundance

In this study, we used the concept of codon abundance to measure the occurance of specific codons in the 50 codons within the 5' or 3' of the coding region. The calculation of codon abundance followed a previous study (Nakamura et al., 2000). To better demonstrate the difference, the final results were presented in the following form:

$$\text{Slope}_{codon_i} = \frac{\text{codon abundance}_{\text{codon}_i,3'} - \text{codon abundance}_{\text{codon}_i,5'}}{codon\ abundance_{\text{codon}_i,5'}}$$

Slope_{codon_i} represents the slope of $codon_i$ in which $\text{codon abundance}_{\text{codon}_i,3'}$ represents the codon abundance of $codon_i$ in the 3' region while $\text{codon aboundance}_{\text{codon}_i,5'}$ represents the codon abundance of $codon_i$ in the 5' region.

Differential translation analysis

Since AltRibo, CanRibo and total ribosomes were collected from the same population of bacteria, to identify differential translated genes we used edgeR on the corresponding ribosome profiling datasets (Robinson et al., 2010). During analysis, replicates were included. Differentially translated genes were identified by $\log_2$fold change (FC) > 0.5(up-regulated) or $\log_2$FC< -0.5(down-regulated) and P value < 0.05. In this study, the datasets of total ribosome were treated as the control and compared against AltRibo or CanRibo to identify differentially translated genes.

Gene ontology analysis

The gene ontology analysis was performed using DavidTools (https://david.ncifcrf.gov). We confined our analysis to those genes with homologues in the better-annotated *M. tuberculosis*-H37Rv genome using high/low gene lists from both strain A and strain B as described above. Top 3 enriched GO categories were presented (Strain A had only 2 GO sets that were enriched in the "high" classification).

Phage stock preparation

Temperature sensitive (Ts) MycoMarT7 phage (Sassetti et al., 2001) was selected for amplifying high-titered phage stock. Serial dilutions of the Ts phage (50µl), mixed with 100µl

MP buffer (50mM Tris, 150mM NaCl, 10mM $MgSO_4$, 2mM $CaCl_2$) and washed stationary *M. smegmatis*, 3.5ml Top agar (0.6% Agar supplied with 2mM CaCl2) and poured on LB plates. Plates were incubated at 30°C for 2 days looking for "Lacy" plates. Once the best concentration of phage where the "lacy" state appeared, 4 more plates were made in the same manner. Each lacy plate was flooded with 3mL MP buffer, gently rocked at 4°C overnight. The Ts phage stock was collcted and filter sterilized (0.2μM filter). The phage stock was tittered and used downstream if, titer was greater than 10^{11}PFU/ml.

Transposon mutagenesis

A 50ml stationary culture of *M. smegmatis* in 7H9 (OD_{600nm} > 6) was grown and then centrifuged at 4500x*g*, 10 min. After discarding the supernatant, the pellet was washed 3 times with MP buffer and resuspended in approximately 5ml of MP buffer. Both the resuspended bacteria and phage stock were warmed to 30°C. Approximately $6x10^{11}$ PFU warmed phage was added to the warmed bacilli and then shaken at 37°C for 4h. Immediately after transduction, ~300-400μl of the transduction mixture was plated on 15cm agar plates, containing 20μg/ml kanamycin and 0.1% Tween80, with or without zinc chelation by TPEN as per the experimental condition. After incubation at 37°C for 3 days, the library size was estimated, and the transductants harvested by scraping the colonies from each plate into 7H9 with 15% glycerol. These were pooled and mixed well before aliquoting and storage at -80°C. For this study, each transposon library comprised at least 100,000 transductants (i.e. individual transposon-mutagenized clones).

Transposon library genomic DNA extraction and sequencing library construction

A library aliquot was centrifuged at 1700x*g* for 10 min, and the supernatant discarded. The bacteria were washed with TE buffer twice and resupended in 400μl ddH_2O, 4μl 1M Tris (pH=9), and 800μl Phenol:Chloroform:Isoamylol (25:24:1) added to the suspension. The bacteria were disrupted by beads beating. Following this, the bacterial lysate was centrifuged at 20800x*g*, 4°C

for 5min. The upper layer was transferred to a new tube, 1.5μl RNaseA added and incubated at 37°C for 1h. After RNaseA digestion, 0.1volume of 3M NaOAc (pH=5.2), 1ml ice-cold ethanol were added to the tube, mixed thoroughly and centrifuged at 20800x*g*, 4°C for 10 min, following which the supernatant was discarded. 40μl 3M NaOAc (pH=5.2), 1ml ice-cold ethanol was added again to the resuspended pellet and centrifuged at 20800x*g*, 4°C for 10 min. The supernatant was discarded, leaving the DNA pellet. The DNA pellet was washed with 70% ethanol, repeating 4-5 times. Finally, the library DNA was resuspended in 200μl ddH_2O.

For each library DNA, 5-10μg genomic DNA was resuspended in 150μl TE and place in a Covaris tube, using the following parameters of a sonicator to fragment the DNA to between 200-500bp: duty cycle (10%), intensity (4), cycles/burst (200), time (80s). The fragmented genomic DNA was purified by AMPure XP beads. The fragmented DNA was further end-repaired by NEBNext Ultra End Repair/dA tailing module by mixing 3μl End prep Enzyme Mix, 6.5μl end repair reaction buffer and 55.5 μl fragmented DNA and incubating at 20°C for 30 min following which 65°C for 30 min. After end repair, 15μl Blunt/TA ligase master mix, 2.5μl annealed adapter mix and 1μl ligation enhancer was added, and incubated at 20°C for 60 min. Adaptor ligated fragmented DNA was further purified by AmpureXP beads. Using the purified DNA as template, the 1st nested PCR was carried out to amplify the fragment containing the transposon junction and adapter by KAPA HiFi HotStart PCR kit. The PCR products were further purified by AmpureXP beads. The 1st nested PCR products were further transferred to a 2nd nested PCR with Illumina sequencing adaptor and index sequence. PCR products were visualized by 2% Agarose gel electrophoresis and PCR products were purified by standard gel purification. The quality of the libraries was examined by an Agilent 2100 Bioanalyzer. Libraries were sequenced on the Illumina X-ten sequencer.

Tn-seq data analysis

Basal reads preparation, mapping to TA sites in the *M. smegmatis* genome assembly and read counts were reduced to unique template counts by TRANSIT tool (DeJesus et al., 2015). Loci that were differentially disrupted were analyzed by using the 'resampling' method in transit, with defalut parameters. During analysis, replicates were included. Genes that were down-represented ($log_2FC < -1$, p-value < 0.05) and over-represented ($log_2FC > 1$, p-value < 0.05) were plotted as shown in Fig. 6.

Statistical Analysis

Appropriate statistical tests are detailed within each protocol and in the figure legends.

Figure 1

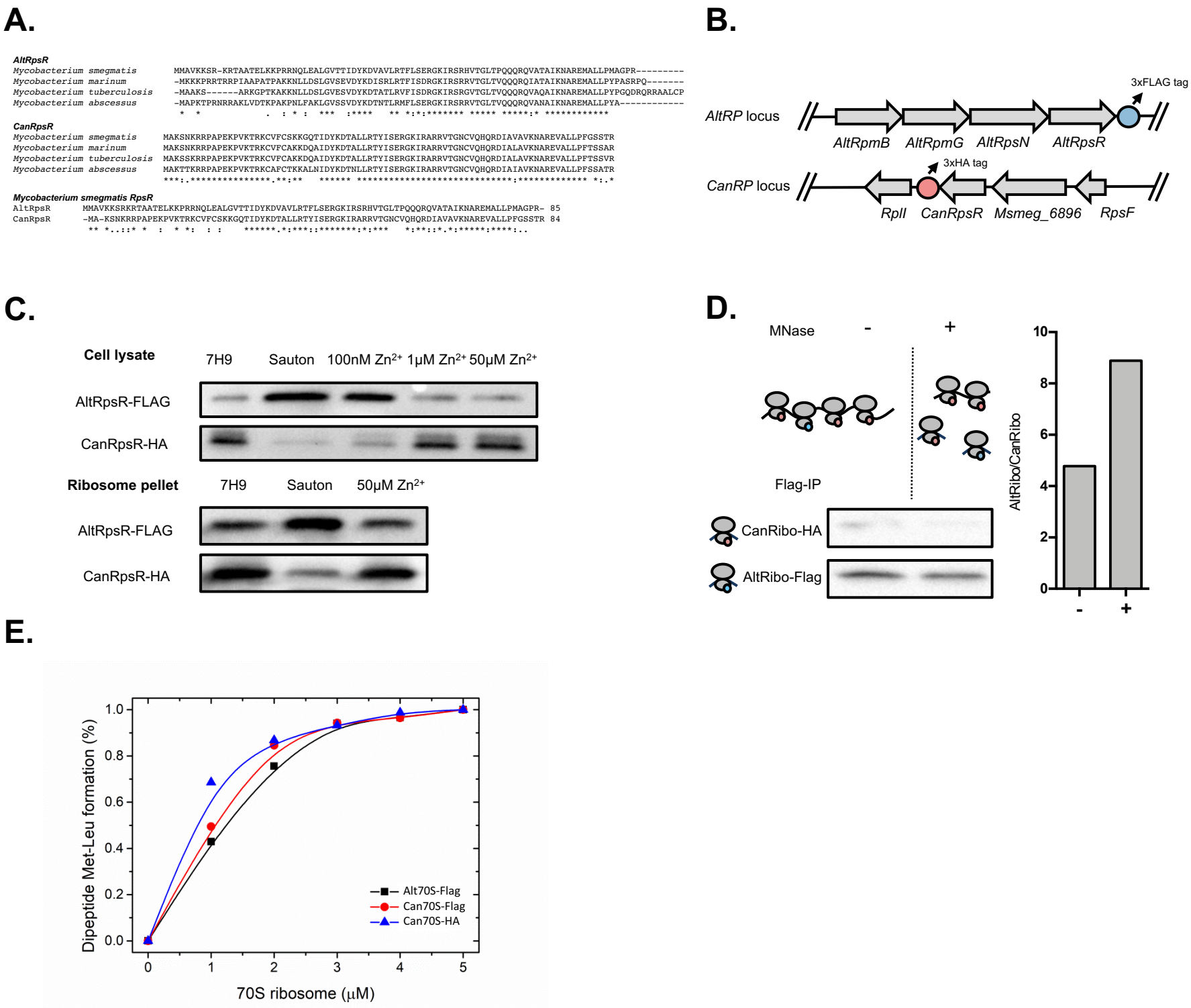

Figure 1. Alternative mycobacterial ribosomes engage in gene translation.
(A) Sequence alignments of AltRpsR and CanRpsR in 4 mycobacterial species (top and middle panels) and the AltRpSR and CanRpsR from *M. smegmatis* (bottom panel).
(B) Cartoon representing the C-terminus affinity tagging of the native CanRpsR and AltRpsR native loci.
(C) Anti-FLAG and anti-HA Western blots of cell lysate (top panel) and of ribosome pellets (bottom panel) in complete 7H9 medium (7H9) and in standard Sauton's medium (Sauton) or Sauton's medium supplemented with zinc sulfate (at indicated concentrations).
(D) Polysomes were isolated and subjected to +/- MNase digestion (cartoon). Following digestion, AltRibos were isolated by FLAG-immunoprecipitation and the fraction blotted with anti-FLAG and anti-HA antibodies. Relative quantification by image analysis of AltRpsR and CanRpsR with our without digestion from the western blots is shown in the histogram.
(E) Di-peptide formation of AltRibos vs CabRibos with a fully reconstituted mycobacterial translation system (Li et al., 2018b). Peptides were detected and analyzed by high performance liquid chromatography (HPLC).

Figure 2

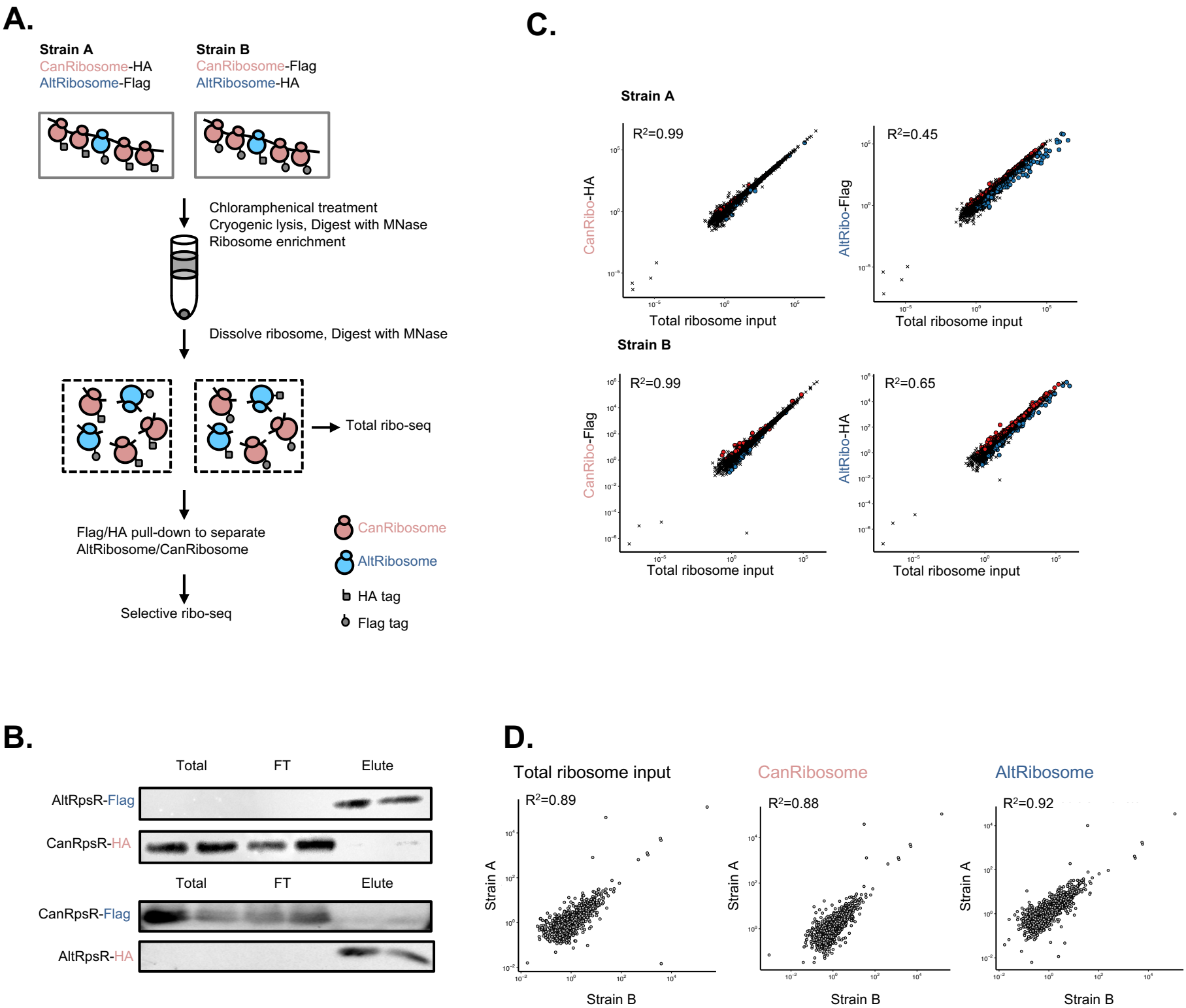

Figure 2. Alternative ribosomes have distinct translational profiles.
(A) Cartoon outlining work-flow for performing selective ribosome profiling in the two RpsR-tagged strains – strain A and strain B (and see Methods).
(B) Western blot against FLAG (AltRibo) and HA (CanRibo) following isolation of ribosomes for ribosome profiling as in (A). Blots from two biological replicates are shown.
(C) Scatter plot showing selective ribosome profiles compared with total ribosome input in Strain A and Strain B. Axes represent reads per kilobase per million mapped reads (RPKM). Blue and red dots represent down- and up-regulated reads respectively (and see Fig. 5A). R^2 represents Pearson correlation.
(D) Correlation of translation efficiency of total ribosome, selective CanRibo and selective AltRibo inputs in Strain A compared with Strain B. R^2 represents Pearson correlation.

Figure 3

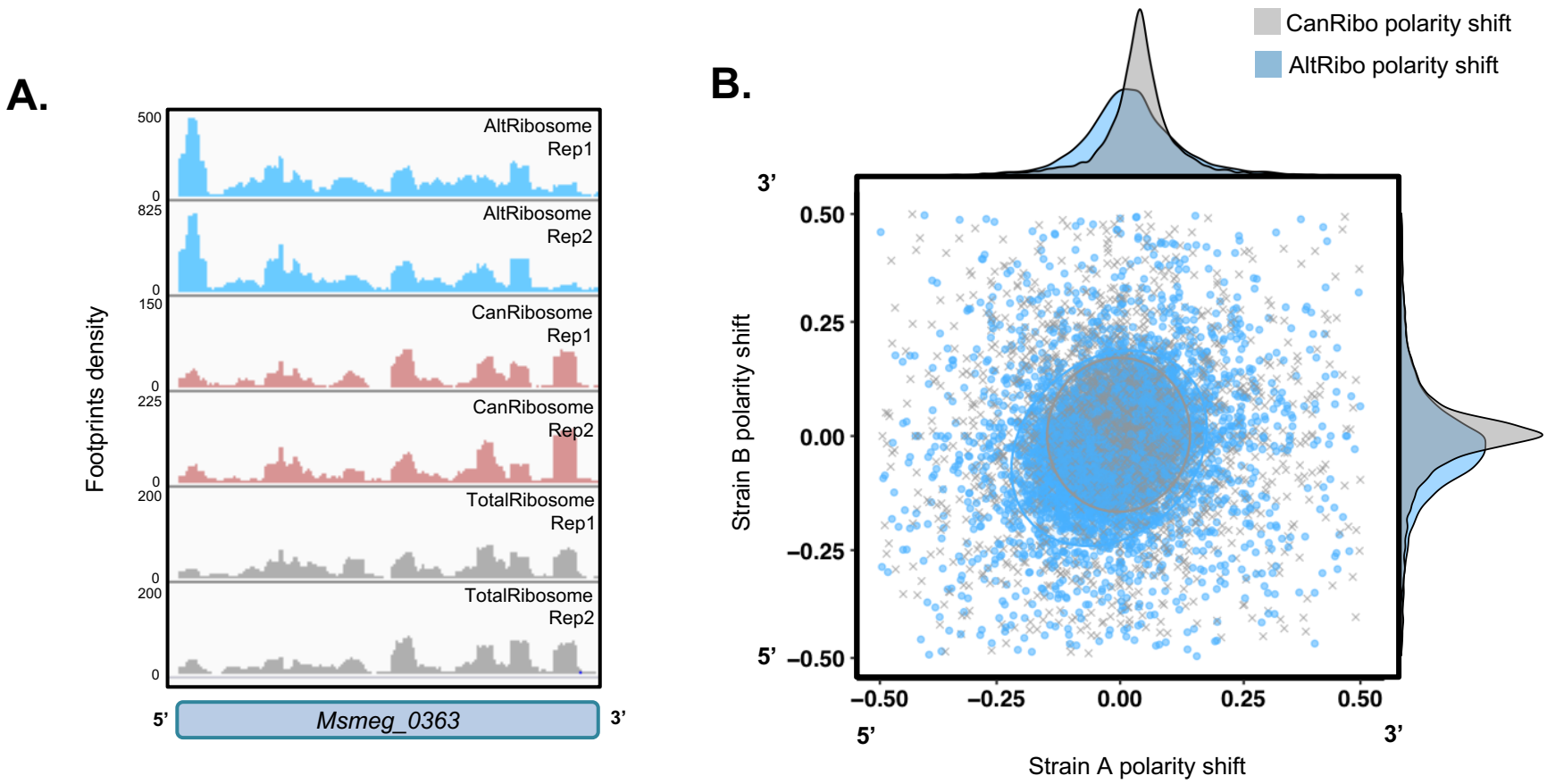

Figure 3. Alternative ribosomes have 5' read accumulation compared with canonical ribosomes.
(A) Normalized reads of each ribosome input for the gene *Msmeg_0363* were plotted along gene length using IGV software (see Methods). Reads from AltRibos show a clear 5' accumulation compared with reads generated from CanRibos or total ribosomal input.
(B) Shifts in polarity scores for the entire genome generated from selective AltRibo and CanRibo reads from Strains A and B – blue dots represent shifts calculated from AltRibos and gray squares represent shifts calculated from CanRibos. The overall polarity score shifts are illustrated as smoothed curves above and to the right of the plot. A negative score indicates 5' read accumulation and a positive score indicates a 3' read accumulation.

Figure 4

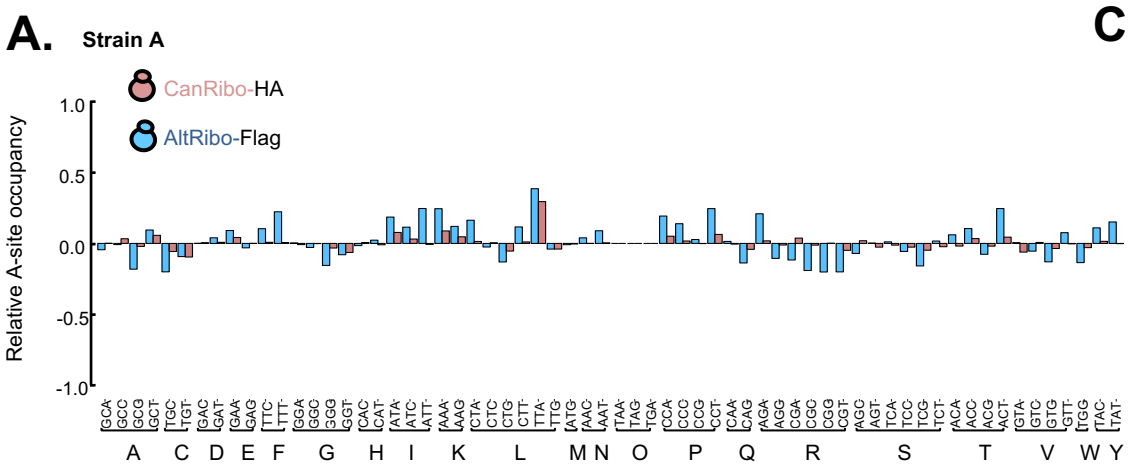

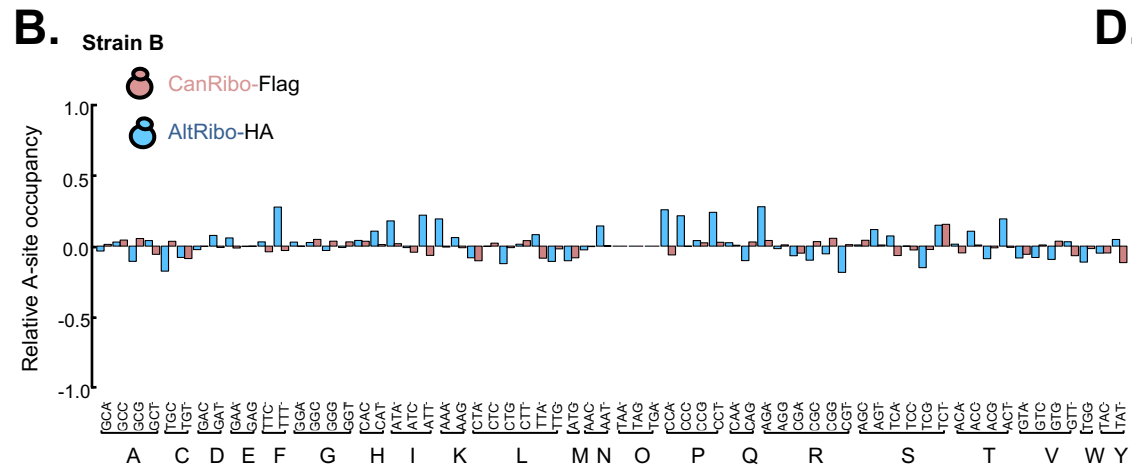

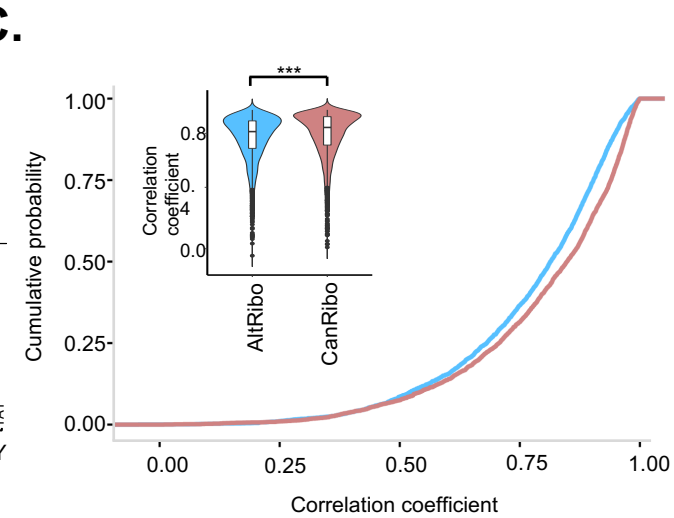

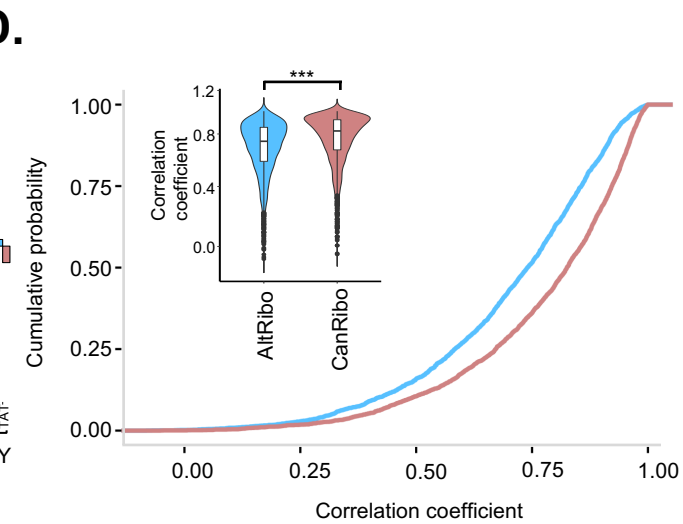

E.

AltRibosome high occupancy codons	AltRibosome low occupancy codons
AAA(K)	ACG(T)
AAG(K)	CAG(Q)
AAT(N)	CGC(R)
ACC(T)	CGG(R)
ACT(T)	CGT(R)
AGA(R)	CTG(L)
ATT(I)	GCG(A)
CCA(P)	GTC(V)
CCC(P)	GTG(V)
CCT(P)	TCG(S)
GAA(E)	TGC(C)
TTT(F)	TGG(W)

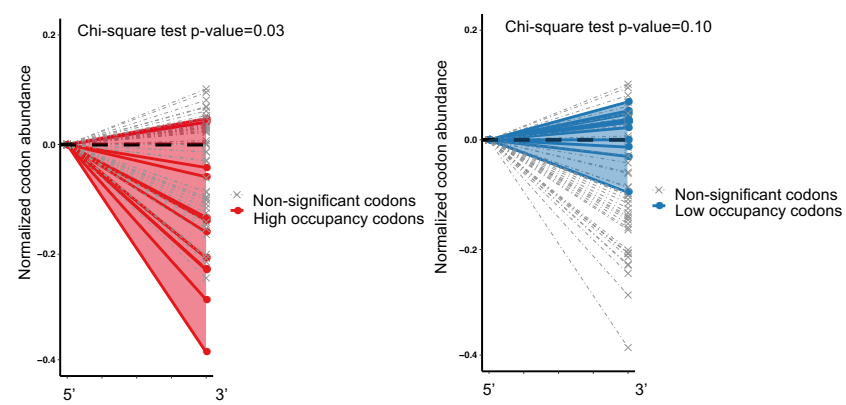

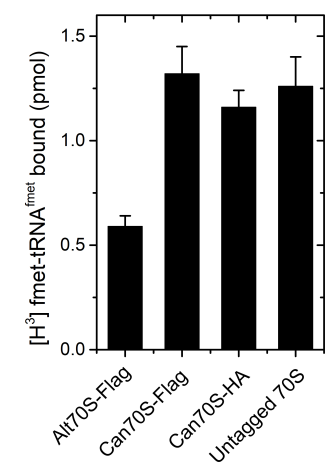

H.

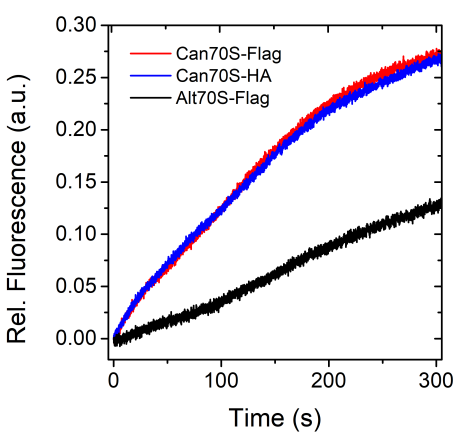

Figure 4. Alternative ribosomes have distinct codon preferences compared with canonical ribosomes.

The relative A-site codon occupancy for all 61 sense codons for AltRibos and CanRibos in Strain A (A) and Strain B (B) compared with total ribosome input. Cumulative probability and violin (inset) plots for correlation between codon occupancy for AltRibos and CanRibos compared with total ribosome input from both Strain A (C) and Strain B (D). *** $p<0.001$ by Student's t-test.

(E) Combining data from Strain A and B, AltRibos have 12 high and 12 low occupancy codons compared with CanRibos.

(F) The relative codon frequencies of the 5' 50 codons and 3' 50 codons for each ORF were analyzed. Comparing AltRibo high occupancy codons (left panel) and low occupancy codons (right panel – both from E above) with non-significantly enriched codons, there was significant enrichment of high occupancy codons at the beginning of ORFs, and a trend towards enrichment of low occupancy codons at the end of ORFs by chi-squared test.

(G) The extent of initiation complex formation by AltRibos compared with CanRibos measured by retention of ^{3}H-fMet count on a nitrocellulose filter (see Methods).

(H) The kinetics and extent of binding of the initiator tRNA to the mRNA programmed 70S ribosome (AltRibo vs CanRibo) followed with BODIPY fluorescence

Figure 5

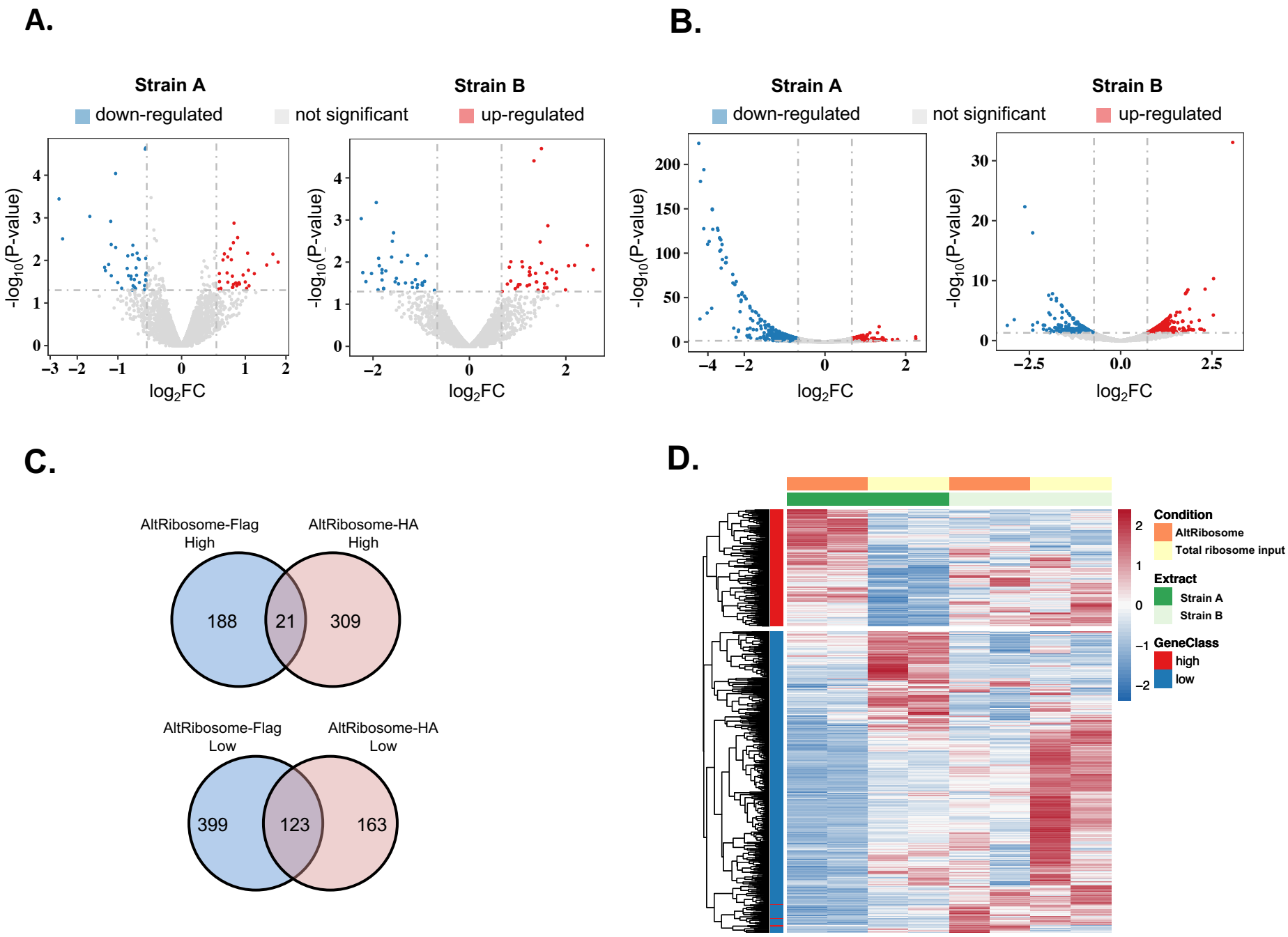

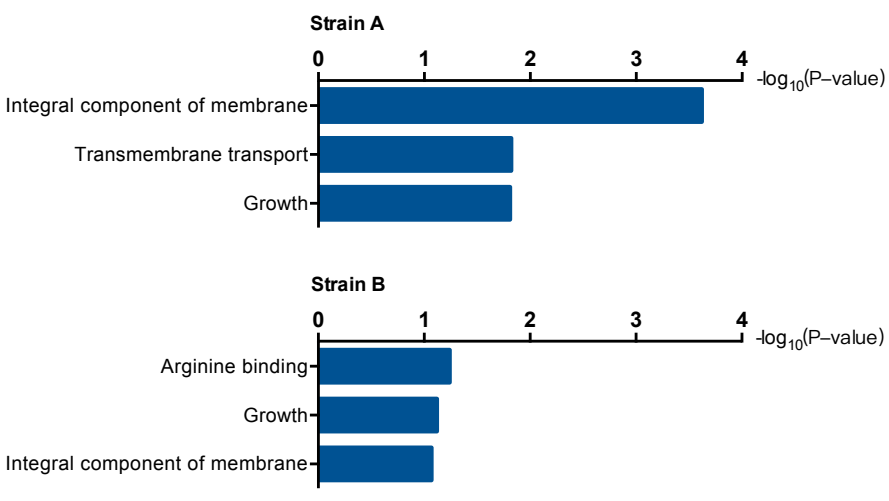

Figure 5. Alternative ribosomes have translational bias for a subset of genes.
Normalized ribosome profile read density for CanRibos (A) and AltRibos (B) compared with total ribosome input in Strain A (left panel) and Strain B (right panel). Significantly upregulated (log_2 fold-change (FC) >0.5, p-value <0.05) and downregulated (log_2 FC<0.5, p-value <0.05) genes are represented by red and blue dots respectively. Degree of overlap in up- and down-regulated genes in the two strains are shown by Venn diagrams (C).
(D) Heatmap of the 209 up- and 522 down-regulated genes by AltRibos, clustered by relative translation efficiency by ribosome profiling from each biological replicate for AltRibos compared with total ribosome input across both strains A and B.
(E) Gene ontology analysis (using DavidTools) of the top three low-enriched translated genes from AltRibos.

Figure 6

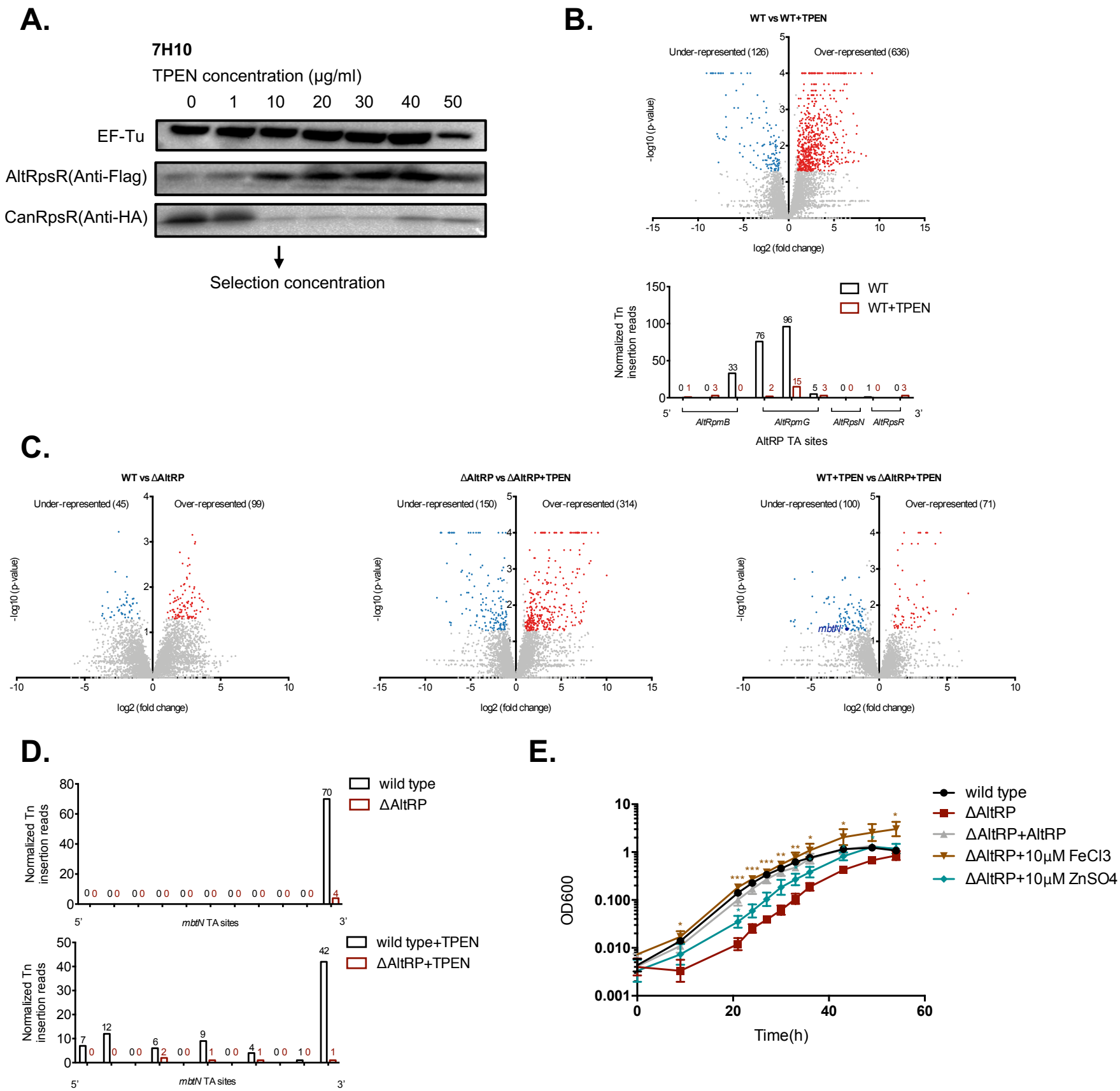

Figure 6. Synthetic lethal interaction analysis reveals a role for the AltRP operon in iron homeostasis.
(A) Western blot against CanRpsR (anti-HA) and AltRpsR (anti-FLAG) for wild-type *M. smegmatis* scraped from 7H10-agar plates supplemented with increasing concentrations of TPEN. Antibody against EF-Tu was used as a loading control.
(B) Upper panel: Volcano plot of fold-change in transposon insertions against p-value by resampling test for Tnseq analysis of wild-type *M. smegmatis* plated without zinc depletion (WT) versus wild-type *M. smegmatis* plated on 7H10-agar supplemented with TPEN (WT+TPEN). Significantly over- and under-represented transposon insertions (p-value <0.05, $\log_2$ FC >1 or $\log_2$ FC <-1 by resampling test) are shown in red and blue respectively. Lower panel: Transposon insertion reads in wild-type *M. smegmatis* plated without zinc depletion (WT) and on 7H10-agar + TPEN (WT+TPEN) for the TA loci in the four AltRP genes. Number of normalized transposon reads per TA locus are shown above the bar graphs.
(C) Volcano plots as in (B) for Tnseq analysis comparing wild-type *M. smegmatis* or *M. smegmatis*-ΔAltRP (ΔAltRP) plated without zinc depletion or on 7H10+TPEN ("+TPEN").
(D) Transposon insertion reads in wild-type *M. smegmatis* or *M. smegmatis*-ΔAltRP (ΔAltRP) plated without zinc depletion and on 7H10-agar + TPEN ("+TPEN") for the TA loci in the gene coding for MbtN. Number of normalized transposon reads per TA locus are shown above the bar graphs.
(E) Growth curve (as measured by OD_{600nm}) in chelated medium for wild-type *M. smegmatis*, *M. smegmatis*-ΔAltRP (ΔAltRP), *M. smegmatis*-ΔAltRP complemented with the AltRP operon (ΔAltRP + AltRP), or *M. smegmatis*-ΔAltRP (ΔAltRP) grown in chelated medium subsequently supplemented with iron (ΔAltRP + 10µM $FeCl_3$) or zinc (ΔAltRP + 10µM $ZnSO_4$). Data show biological triplicates +/- SD and results are representative of two independent experiments. * p<0.05, ** p<0.01, *** p<0.001 by Student's t-test. Brown asterisks represent comparison between ΔAltRP and ΔAltRP+10µM $FeCl_3$, green asterisks represent comparison between ΔAltRP and ΔAltRP+10µM $ZnSO_4$.